Systemic immune dynamics in cancer

Bakker, E.A.M.

Citation

Bakker, E. A. M. (2026, January 9). *Systemic immune dynamics in cancer*. Retrieved from https://hdl.handle.net/1887/4286248

IL-5-producing CD4+ T cells and eosinophils cooperate to enhance response to immune checkpoint blockade in breast cancer

Olga S. Blomberg[1,2,3,*], Lorenzo Spagnuolo[1,2,*], Hannah Garner[1,2,*], Leonie Voorwerk[1,*], Olga I. Isaeva[1,4,**], Ewald van Dyk[1,2,4,**], Noor Bakker[1,2,**], Myriam Chalabi[5,6,7], Chris Klaver[1], Maxime Duijst[1], Kelly Kersten[1,11], Marieke Brüggemann[1], Dorien Pastoors[1,2,12], Cheei-Sing Hau[1,2], Kim Vrijland[1,2], Elisabeth A.M. Raeven[1,2], Daphne Kaldenbach[1,2], Kevin Kos[1,2,3], Inna S. Afonina[8,9], Paulien Kaptein[5], Louisa Hoes[2,5,7], Willemijn S.M.E. Theelen[10], Paul Baas[10], Emile E. Voest[2,5,7], Rudi Beyaert[8,9], Daniela S. Thommen[5], Lodewyk F.A. Wessels[2,4], Karin E. de Visser[1,2,3,***,#], and Marleen Kok[1,7,***]

[1] Division of Tumor Biology & Immunology, The Netherlands Cancer Institute, Amsterdam, the Netherlands
[2] Oncode Institute, Utrecht, the Netherlands
[3] Department of Immunology, Leiden University Medical Centre, Leiden, the Netherlands
[4] Division of Molecular Carcinogenesis, The Netherlands Cancer Institute
[5] Division of Molecular Oncology & Immunology, The Netherlands Cancer Institute
[6] Department of Gastrointestinal Oncology, The Netherlands Cancer Institute
[7] Department of Medical Oncology, Netherlands Cancer Institute
[8] VIB-UGent Center for Inflammation Research, Ghent University, Ghent, Belgium
[9] Department of Biomedical Molecular Biology, Ghent University, Ghent, Belgium
[10] Department of Thoracic Oncology, Netherlands Cancer Institute
[11] Present address: Department of Pathology, University of California San Francisco, San Francisco, CA, USA
[12] Present address: Department of Hematology, Erasmus University Medical Center, Rotterdam, the Netherlands

*These authors contributed equally
**These authors contributed equally
***These authors contributed equally, co-corresponding authors
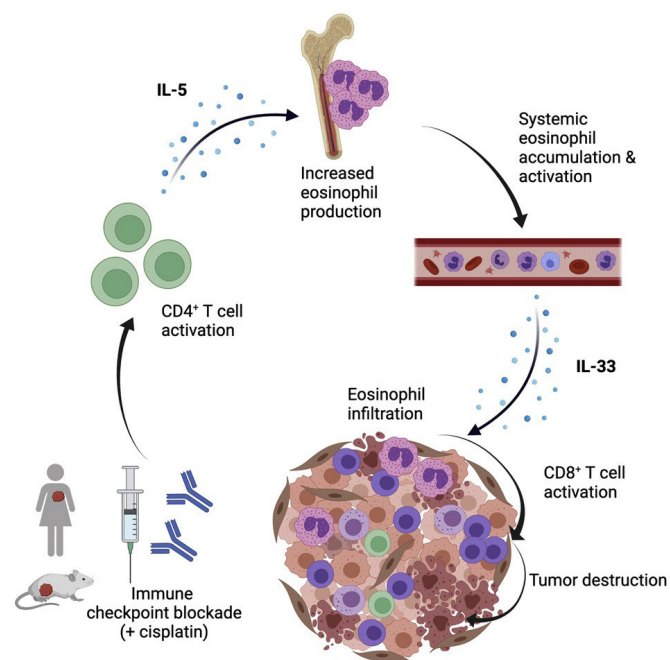#Lead contact

Summary

Immune checkpoint blockade (ICB) has heralded a new era in cancer therapy. Research into the mechanisms underlying response to ICB has predominantly focused on T cells, however effective immune responses require tightly regulated crosstalk between innate and adaptive immune cells. Here, we combine unbiased analysis of blood and tumors from metastatic breast cancer patients treated with ICB with mechanistic studies in mouse models of breast cancer. We observe an increase in systemic and intratumoral eosinophils in patients and mice responding to ICB treatment. Mechanistically, ICB increased IL-5 production by CD4+ T cells, stimulating elevated eosinophil production from the bone marrow, leading to systemic eosinophil expansion. Additional induction of IL-33 by ICB-cisplatin combination or recombinant IL-33 promotes intratumoral eosinophil infiltration and eosinophil-dependent CD8+ T cell activation to enhance ICB response. This work demonstrates the critical role of eosinophils in ICB response and provides proof-of-principle for eosinophil engagement to enhance ICB efficacy.

Keywords

Eosinophils, breast cancer, immune checkpoint blockade, myeloid cells, IL-5, CD4+ T cells, IL-33

Graphical Abstract

Introduction

Immune checkpoint blockade (ICB) has emerged in the last decade as an effective strategy for the treatment of multiple cancer types. However, in metastatic breast cancer, durable responses are only seen in approximately 5% of the patients and are mainly limited to triple-negative breast cancer (TNBC)[1,2]. Whilst response rates can be increased by selecting patients with PD-L1-positive tumors or by combining ICB with chemotherapy[3,4], most breast cancer patients do not benefit from ICB. A better understanding of the mechanisms that underlie response to ICB is crucial for the rational design of novel immunomodulatory strategies.

Research into the mechanisms of response to ICB has predominantly focused on T cells, however, an effective immune response requires tightly regulated crosstalk between adaptive and innate immune cells[5]. One innate immune cell type gaining increasing attention in the context of anti-tumor immunity is the eosinophil[6,7]. Eosinophils are bone marrow-derived granulocytes involved in tissue homeostasis and repair, parasite clearance and the pathophysiology of various diseases, including allergic asthma and autoimmunity[8]. In the context of cancer, opposing functions of eosinophils have been reported depending on cancer type and disease stage[9-18]. Recently, eosinophils have emerged as unexpected players in an effective response to ICB. Increased eosinophil levels during ICB treatment correlate with response to PD-1, PD-L1 or CTLA-4 targeting antibodies in patients with metastatic melanoma[19-21], non-small cell lung cancer (NSCLC)[22,23] and renal cell carcinoma (RCC)[24]. Whether eosinophils are associated with response to ICB in patients with less immunogenic cancer types, such as breast cancer, remains to be elucidated. Moreover, it is critical to assess whether eosinophils merely serve as a biomarker or are causally involved in ICB response. Preclinical studies point towards a functional involvement of eosinophils in anti-tumor immunity[11-14] and eosinophils were also recently reported to promote intratumoral vessel normalization and anti-tumor immunity upon CTLA-4 blockade[25]. Nonetheless, their role in ICB response remains poorly understood. Furthermore, the mechanisms leading to eosinophil accumulation and recruitment to the tumor upon ICB are still unknown.

In this study, we combined unbiased analyses of the systemic immune landscape upon ICB in patients with metastatic TNBC with in-depth mechanistic studies in spontaneous mouse models of primary and metastatic breast cancer (Figure 1A), which mimic the poorly immunogenic and highly immunosuppressive characteristics of human breast cancer[26,27]. We uncover a critical role for eosinophils during ICB response and elucidate the mechanisms that lead to systemic eosinophil expansion and tumor infiltration.
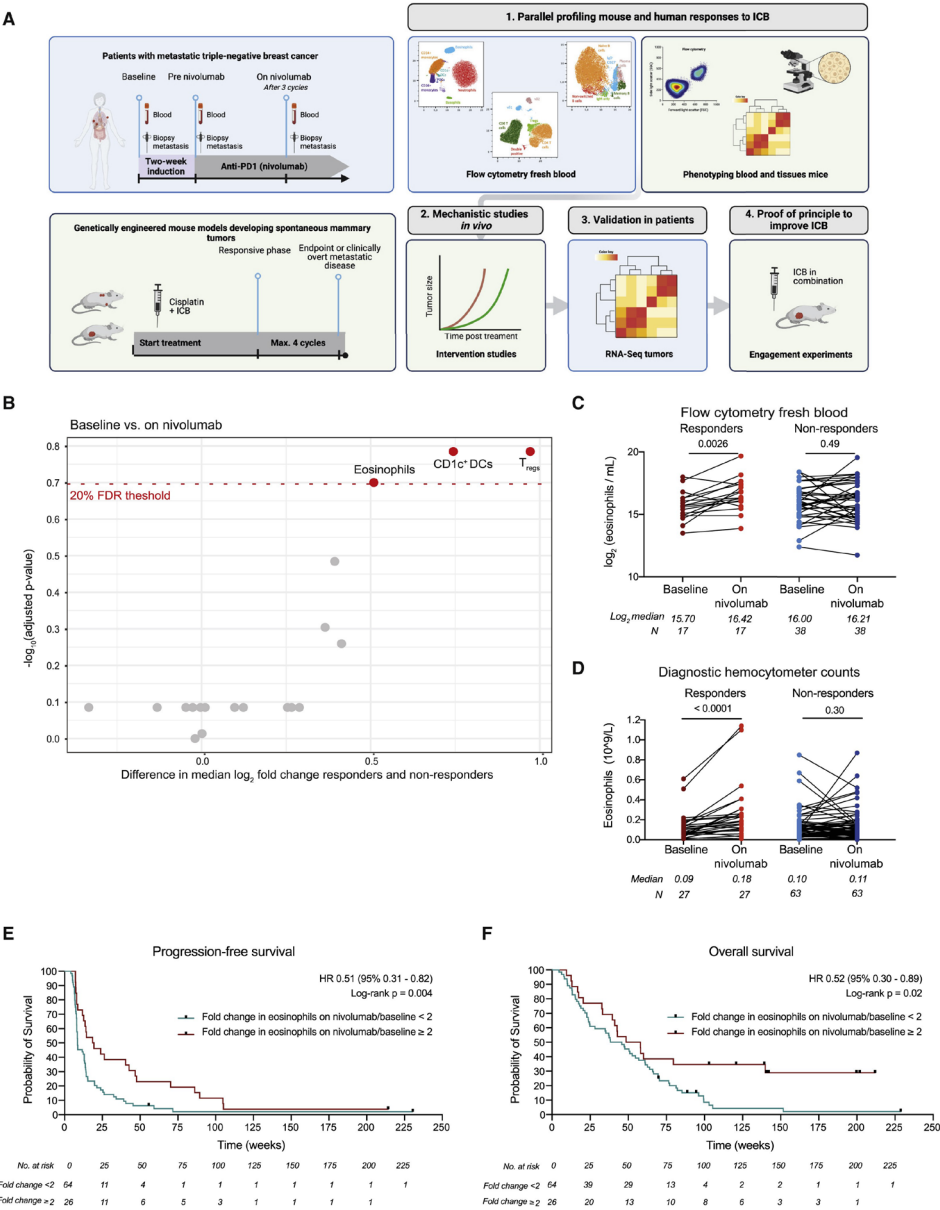
Figure 1. ICB response in metastatic TNBC patients is associated with systemic eosinophil expansion. *(A) Schematic overview of study design. Created with Biorender.com. (B) Volcano plot depicting the difference in median log$_2$ fold change from baseline to on-nivolumab between responding and non-responding TNBC patients with metastatic TNBC (TONIC-trial, NCT02499367) and adjusted p-values for systemic immune cell populations (cells/ml) analyzed by flow cytometry. (C-D) Paired analysis of circulating eosinophils at baseline versus on-nivolumab by flow cytometry (log$_2$ transformed cells/ml) (C) and by hemocytometer analysis (D). Wilcoxon Signed-Rank test.*

(E-F) Kaplan-Meier curve of progression-free survival (E) or overall survival (F) of patients according to the fold change in eosinophils (baseline to on-nivolumab) lower than 2 or equal to/higher than 2. Log-rank and univariate hazard ratios by Cox regression (fold change lower than 2 as reference category). See also Figures S1-S3 and Tables S1-S2.

Results

Increase in circulating eosinophils in patients responding to ICB

To assess response-related changes in the systemic immune landscape of patients with metastatic breast cancer, we set up an immunomonitoring pipeline of fresh blood by high-dimensional flow cytometry (Figure 1A). We profiled patients with metastatic TNBC treated with anti-PD-1 (nivolumab) enrolled in a phase II clinical trial (TONIC-trial, n=111, Figure S1A-B; characteristics in Table S1-S2)[28]. Patients were treated with nivolumab alone or with nivolumab following a two-week induction period with either low dose chemotherapy, irradiation or a two-week waiting period (Figure S1A). Blood samples were analyzed by flow cytometry at baseline (before induction treatment), after induction treatment (pre-nivolumab) and after three cycles of nivolumab (on-nivolumab). Extensive analysis of individual timepoints did not reveal predictive immune cell populations that could distinguish responders from non-responders (Figure S1C-E). However, when analyzing the dynamics of immune cell populations upon ICB treatment by comparing baseline to on-nivolumab, we identified three differentially regulated immune cell populations associated with response: CD1c+ dendritic cells (DCs), regulatory T cells (T$_{regs}$) and eosinophils (Figure 1B & S1F). We observed a decrease in CD1c+ DCs in non-responding patients (Figure S2A). In contrast, eosinophils and T$_{regs}$ were increased upon ICB specifically in responders (Figure 1C & S2B-C). The same three populations emerged when we compared the pre-nivolumab (post-induction) to on-nivolumab timepoints, indicating that the induction treatments did not significantly change the dynamics of these immune populations (Figure S2D-F). In light of recent reports of systemic eosinophil expansion correlating with ICB response in several tumor types[19-24], we further investigated the increase in eosinophils associated with response to ICB.

To validate our results in a technically independent manner we evaluated circulating eosinophil counts using routine hemocytometer analysis (Figure S1B for sample overlap with flow cytometry samples). We confirmed circulating eosinophils significantly increase in responders on-nivolumab, both compared to baseline and pre-nivolumab (Figure 1D & S2G-H). Importantly, patients with increased circulating eosinophils upon treatment had longer progression-free survival (Figure 1E & S2I) and overall survival (Figure 1F & S2J), underscoring the clinical relevance of an eosinophil increase in ICB response.

To evaluate whether increased eosinophils during ICB response extend beyond breast cancer, NSCLC[22,23], RCC[24] and melanoma[19-21], we investigated eosinophil counts in patients

7

treated with ICB in other phase II clinical trials at the Netherlands Cancer Institute. Comparing patients responding to ICB with non-responders, we observed a significantly higher fold change in circulating eosinophils in patients with advanced NSCLC (Figure S3A,B; PEMBRO-RT trial[29]) and in patients with early stage mismatch repair-proficient (pMMR) colon cancer (CC) (Figure S3C,D; NICHE-trial[30]). No statistically significant difference in paired eosinophil counts could be seen upon ICB in patients with mismatch repair-deficient (dMMR) cancers (Figure S3E,G; NICHE-trial and dMMR cohort DRUP-trial[30,31]), suggesting that an eosinophil increase might be less relevant in highly immunogenic tumors. In summary, we demonstrate that eosinophils accumulate systemically upon ICB response in three independent cohorts of patients with metastatic TNBC, metastatic NSCLC or early-stage pMMR CC, emphasizing that systemic eosinophil expansion is a common feature of ICB response across multiple cancer types.

Increase of intratumoral eosinophil-related gene expression correlates with response to ICB and increased CD8+ T cell signatures
To assess whether eosinophils accumulate intratumorally upon ICB, we evaluated the expression of *SIGLEC8* in paired metastases obtained at baseline and during nivolumab treatment of TNBC patients (TONIC-trial, NanoString IO360 panel, sample availability Figure S1B). SIGLEC8 is a marker expressed at high levels on human eosinophils and mast cells and to a lower degree on basophils[32]. We detected a statistically significant increase in *SIGLEC8* upon ICB in tumors from responders but not in non-responders (Figure 2A). To complement this analysis, we applied an eosinophil signature containing genes highly expressed by eosinophils to the RNA-sequencing dataset (Table S3). Intratumoral expression of these genes increased upon ICB in responders but not in non-responders (Figure 2B). Using this signature, we assessed whether elevation in intratumoral eosinophils is accompanied by an intratumoral increase in (activated) CD8+ T cells, as shown for metastatic melanoma[19]. We applied a widely used T cell inflamed gene signature[33], an IFNg signature[33] and a structural CD8+ T cell signature consisting of genes related to the CD8+ T cell receptor complex (Table S3*)*. We observed a significant correlation between increased expression upon ICB of eosinophil-related genes and all three T cell-related gene signatures in metastatic lesions of responders, and not in non-responders (Figure 2C-H). Together, our results indicate that response to ICB associates with an increase in circulating eosinophils and an increase of eosinophil-related genes in the tumor microenvironment. This increase in eosinophil-related genes correlates with increased CD8+ T cell related genes, suggesting a potential connection between eosinophils and CD8+ T cell activation during an effective ICB response.

ICB synergizes with cisplatin and induces eosinophil accumulation in spontaneous primary and metastatic breast cancer models
Our clinical observations raise the question whether eosinophil expansion is a bystander effect of ICB response, or whether eosinophils are functionally involved. To probe the causality between eosinophil dynamics and outcome after ICB in breast cancer, we used the *Keratin14-cre;Cdh1^{F/F};Trp53^{F/F}* (KEP) mouse model for *de novo* mammary tumorigenesis[34] (Figure 3A) and the KEP-based mastectomy model for spontaneous multi-organ metastatic disease[35] (Figure 3B & S4A,B). KEP mice bearing established mammary tumors did not respond to blockade of PD-1 and CTLA-4 (referred to as ICB; Figure 3C). Similarly, metastasis-bearing mice did not respond to ICB alone (Figure 3D), recapitulating the poor response to ICB observed in metastatic breast cancer patients. Platinum-based drugs synergize with ICB in preclinical models[36,37] due to their beneficial immunomodulatory effects[38,39], in line with improved response rates when ICB is combined with chemotherapy in metastatic TNBC patients[3,4]. While combining cisplatin with either anti-PD-1 or anti-CTLA-4 was insufficient to improve the survival benefit provided by cisplatin (Figure S4C), the combination of cisplatin with anti-PD-1 and anti-CTLA-4 (CIS+ICB) resulted in extension of survival of KEP mice (Figure 3C) and led to durable responses in mice bearing established metastases (Figure 3D). The therapeutic synergy between CIS+ICB was characterized by a systemic increase in effector CD44+CD62L- T cells and increased expression of activation markers and cytokines, such as IFNγ and TNFα by both CD4+ and CD8+ T cells (Figure S4D,E). Depletion of CD8+ T cells abrogated the synergistic effect observed upon CIS+ICB in mammary tumor-bearing KEP mice (Figure 3C), confirming a critical role of CD8+ T cells as effector cells in CIS+ICB therapy.

In addition to increased T cell activation, in-depth profiling of the immune landscape of primary tumors, metastases, and blood by flow cytometry of both models revealed that only eosinophils consistently increased in frequency upon CIS+ICB therapy (Figure 3E-H). Whilst ICB induced accumulation of circulating eosinophils (Figure 3E,F), increased eosinophil infiltration in primary tumors and metastatic lesions was only observed when ICB was combined with cisplatin (Figure G,H). Additionally, we observed an increase in eosinophils in the tumor-draining lymph node (TDLN) and spleen of KEP mice treated with CIS+ICB (Figure S4F). Immunohistochemical staining for Major Basic Protein (MBP), a granular protein specifically expressed by eosinophils, confirmed that the increase in eosinophils in primary KEP tumors was only achieved upon CIS+ICB (Figure S4G).
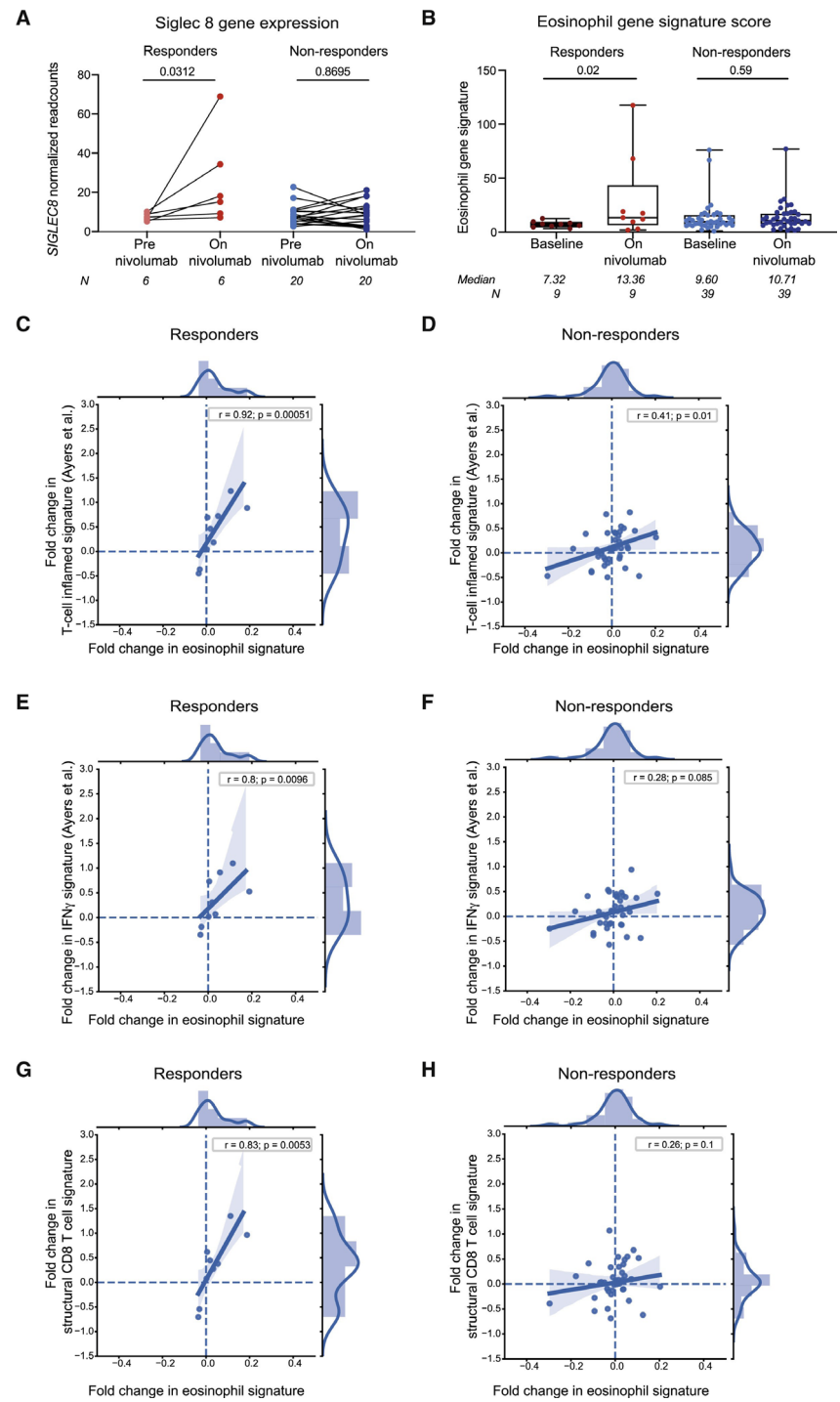
7

◀◀◀ *Figure 2. ICB response in TNBC patients is associated with increased intratumoral eosinophil-related gene expression.* (A) Paired intratumoral SIGLEC8 normalized read counts from NanoString IO360 gene expression analysis from pre-nivolumab and on-nivolumab biopsies. Wilcoxon Signed-Rank test. (B) Mean of normalized expression values of eosinophil signature genes (Table S3) from paired biopsies of metastases as assessed by RNA-sequencing analysis. Boxplots display minimum and maximum values (whiskers), interquartile range (box) with median. Wilcoxon Signed-Rank test. (C-H) Correlation between the fold change (baseline to on-nivolumab) in an eosinophil gene signature (described in B) and the fold change (baseline to on-nivolumab) in a T cell inflamed gene signature (expanded immune gene signature of Ayers et al., 2017[33] (C,D), a structural CD8+ T cell gene signature (Table S3) (E,F), or an IFNg gene signature[33] (G,H) in responders (left) and non-responders (right). Lines with colored field represent the regression line with 95% confidence interval, including histogram and kernel density estimates. Spearman's correlation coefficient. See also Table S3.

To evaluate whether treatment with CIS+ICB also influences the phenotype of eosinophils, we performed RNA-sequencing on eosinophils sorted from blood of metastasis-bearing mice during the responsive phase of therapy, namely 21 days after initiation of treatment. We observed 858 differentially expressed genes (fold change ≥1 and p-value ≤ 0.05) in eosinophils from CIS+ICB-treated mice compared to control antibody-treated mice (Figure S4H). Gene-set enrichment analysis identified IFNγ response as the top hit among the immune-related pathways enriched in eosinophils upon CIS+ICB (Figure S4I-J). Other immune-related pathways included TGFβ signaling, TNFα signaling via NF-κB, IL6-JAK-STAT3 signaling, and inflammatory response (Figure S4I). Moreover, we observed enrichment of oxidative phosphorylation pathway in eosinophils from control antibody-treated compared to combination-treated mice (Figure S4K). These observations indicate that, in CIS+ICB-treated mice, eosinophils are not only increased in number, but also phenotypically altered. Collectively, these data demonstrate that ICB synergizes with cisplatin resulting in improved survival and is associated with systemic and intratumoral expansion of eosinophils, in line with our clinical observations.

Eosinophil depletion abrogates CD8+ T cell activation and ICB response

To elucidate whether CIS+ICB-induced eosinophilia is critical for the observed therapeutic benefit, we depleted eosinophils with an antibody targeting SiglecF[11,12,25,40,41]. Anti-SiglecF treatment effectively depleted eosinophils without altering other immune cells including neutrophils (Figure S5A-C). In line with literature[42], we observed a subset of SiglecF+ neutrophils in our tumor models (5-20% of intratumoral neutrophils, data not shown). However, the expression levels of SiglecF on these neutrophils was lower than on eosinophils (Figure S5D). To exclude the possibility that anti-SiglecF treatment depletes SiglecF+ neutrophils, we quantified Ly6G+ (neutrophils) and MBP+ (eosinophils) cells by immunohistochemical staining. The total number of neutrophils was unaffected by anti-SiglecF treatment, whereas eosinophils were effectively depleted (Figure S5E,F). Importantly, eosinophils were also effectively depleted during anti-SiglecF treatment in combination with cisplatin+/-ICB (Figure 4A & S5G).
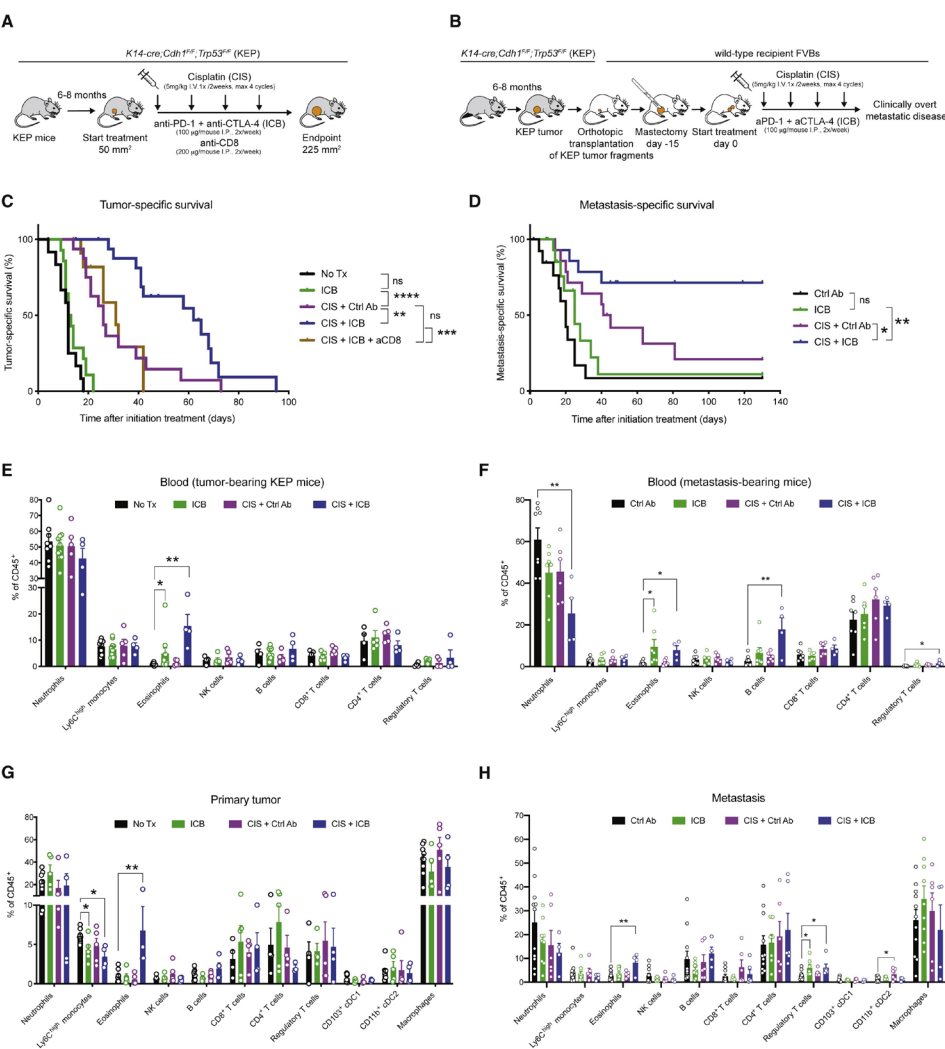
Figure 3. ICB synergizes with cisplatin and induces eosinophil expansion in mouse models.
(A-B) Experimental set-up of transgenic KEP model (A) and KEP-based metastasis model (B) including treatment schemes.(C) Kaplan-Meier survival curves of KEP mice treated as indicated (untreated, No Tx, n=12; ICB, n=14, 1 censored; CIS+Ctrl Ab, n=17, 2 censored; CIS+ICB, n=18, 5 censored; CIS+ICB+anti-CD8, n=12, 4 censored). Tumor-related endpoint was defined as cumulative tumor burden of 225 mm². (D) Kaplan-Meier survival curves of metastasis-bearing mice treated as indicated (control antibody, Ctrl Ab, n=13, 1 censored; ICB, n=15, 5 censored; CIS+Ctrl Ab, n=15, 3 censored; CIS+ICB, n=16, 7 censored). Metastasis-related endpoint was defined as mice displaying signs of respiratory distress caused by metastatic disease or when lymph node metastasis reached the size of 225mm². Censored events are mice sacrificed for weight loss (C&D) or local recurrence of the mastectomized tumor (D). Log-rank (Mantel Cox) test. (E-F) Frequency of immune cell populations in the blood of KEP mice at tumor-related endpoint (E) or metastasis-

bearing mice at metastasis-related endpoint (F) as determined by flow cytometry. (G-H) Frequency of immune cell populations in the primary tumor of KEP mice at tumor-related endpoint (G) or metastatic lesions of mice at metastasis-related endpoint (H) as determined by flow cytometry. Eosinophils were defined CD11b+Ly6G^low SiglecF+SSC^high in blood and CD11b+Ly6G^low SiglecF+F4/80^int in tumor. Mean ±S.E.M.. 1-way ANOVA or Kruskal-Wallis followed by Dunnett's or Dunn's multiple comparisons test, comparing each group against control-treated mice. *p<0.05, **p<0.01, ***p<0.001, ****p<0.0001. See also Figure S4.

The administration of anti-SiglecF alone did not affect KEP tumor growth (Figure S5H). Strikingly, depletion of eosinophils abrogated the synergistic effect observed between CIS+ICB, while depletion of eosinophils had no effect on therapeutic benefit of cisplatin alone (Figure 4B-D). Similarly, depletion of eosinophils completely abrogated the synergistic effect of CIS+ICB in metastasis-bearing mice but had no effect on the efficacy of cisplatin alone (Figure 4E). These findings reveal a causal role for eosinophils in the synergistic effect of CIS+ICB therapy, both in primary and metastatic breast cancer models.

Because the synergistic effect of CIS+ICB is dependent on both CD8+ T cells and eosinophils, we hypothesized that eosinophils play a role in inducing intratumoral CD8+ T cell infiltration or activation. It was previously shown that eosinophils can promote T cell activation and recruitment into tumors[11,13,18,25,40], and we observed an association between intratumoral eosinophils and CD8+ T cells in responding patients with advanced breast cancer (Fig 2C-H). To test this hypothesis, we analyzed the immune landscape of KEP tumors during the responsive phase of therapy. Intratumoral CD8 counts increased upon treatment with cisplatin compared to control antibody but did not further increase upon addition of ICB. Importantly, CD8 counts were not dependent on the presence of eosinophils (Figure 4F). Instead, eosinophil depletion completely reverted the increased activation of intratumoral CD8+ T cells induced by CIS+ICB, most notably in terms of CD44 expression and IFNy production (Figure 4G,H). These data demonstrate that eosinophils are essential for increased intratumoral CD8+ T cell activation during CIS+ICB therapy.

Additionally, CD4 and FOXP3 cell counts increased upon cisplatin treatment compared to control, but did not change further upon CIS+ICB and was independent of eosinophil presence (Figure S5I,J). While CIS+ICB also increased the intratumoral frequency of effector CD44+ CD4+ T cells, this was independent of eosinophils (Figure S5K-N), demonstrating that eosinophils specifically affect intratumoral CD8+ T cell activation. Interestingly, we also observed a higher frequency of CD44+ and IFNy+ CD8+ T cells in the TDLN upon CIS+ICB that was abrogated upon eosinophil depletion (Figure S5O). In contrast, the frequency of CD44+ CD4+ T cells or CD44+ T_regs in TDLN was not increased by combination treatment nor affected by eosinophil depletion (Figure S5P,Q). Collectively, these observations show that eosinophils are critical for the therapeutic action of CIS+ICB, by facilitating CD8+ T cell activation in the tumor and TDLN.
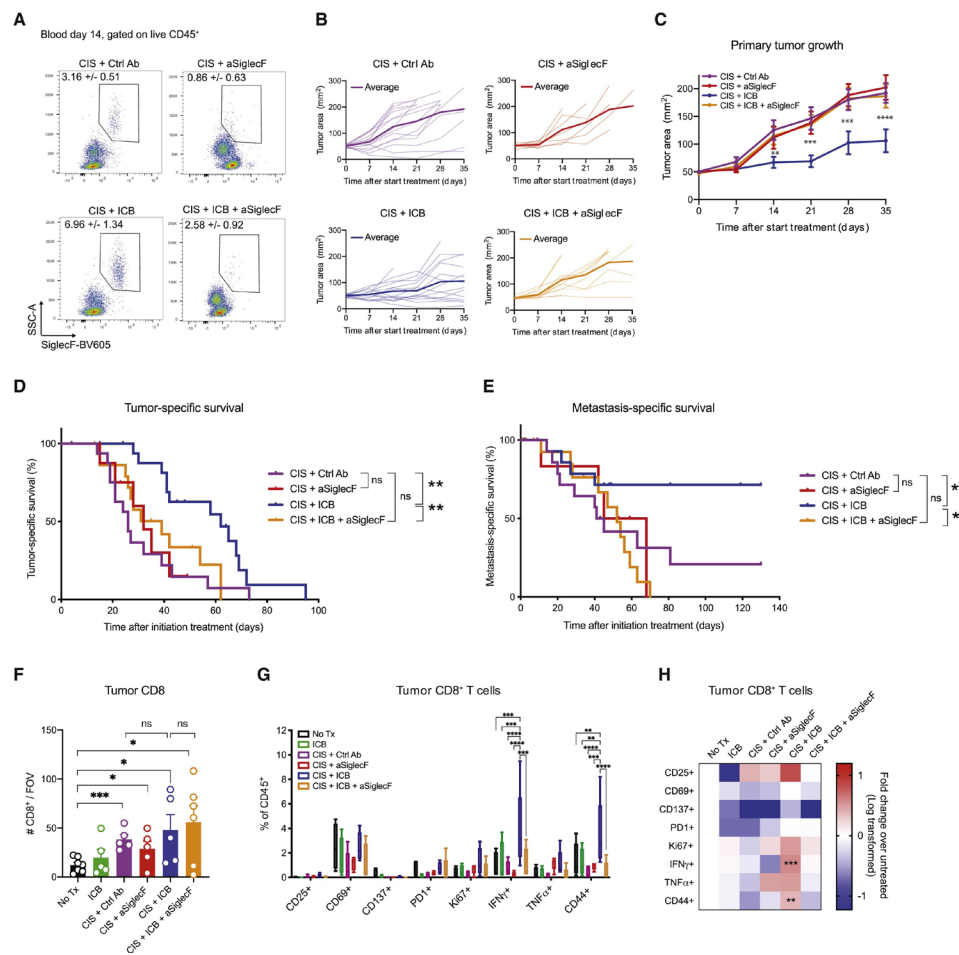
7

Figure 4. Eosinophils are critical for ICB-cisplatin response via CD8+ T cell activation. *(A) Representative dot plots showing eosinophil levels in blood of KEP mice 14 days after start of indicated treatments. Mean frequency of eosinophils as percentage of CD45+ cells ±S.E.M. is displayed. (B) Individual (light) and average (dark) tumor growth curves of KEP mice treated as indicated. (C) Average growth curve ±S.E.M. of the aforementioned treatment groups. 2-way ANOVA followed by Dunnett's multiple comparisons test. (D) Kaplan-Meier survival curves of KEP mice treated as indicated (CIS+Ctrl Ab, same curve as in Figure 3C); CIS+anti-SiglecF, n=8, 2 censored; CIS+ICB, same curve as in Figure 3C; CIS+ICB+anti-SiglecF, n=18, 5 censored). Log-rank (Mantel-Cox) test. (E) Kaplan-Meier survival curves showing metastasis-related survival of mice treated as indicated (CIS+Ctrl Ab, same curve as in Figure 3D; CIS+anti-SiglecF, n=6, 2 censored, CIS+ICB, same curve as in Figure 3D; CIS+ICB + anti-SiglecF, n=19, 7 censored). Log-rank (Mantel-Cox) test. (F) Number of tumor-infiltrating CD8+ T cells quantified by IHC (n=5-7 mice per group, average of 5-9 high power microscopic fields per mouse). KEP mice were treated as described in Figure 3A and analyzed 21 days after start of treatment or when tumors reached an area of 225 mm². Mean ±S.E.M. Student's t-test. (G) Frequency of indicated activation markers expressed on*

intratumoral CD8+ T cells upon different treatments, determined by flow cytometry (n=4-5). Boxes represent median and interquartile range; whiskers full range. 2-way ANOVA followed by Tukey's multiple comparison test. (H) Data of (G) was normalized to the frequency observed in control mice. Log transformed data is presented. ns, not significant, *p<0.05, **p<0.01, ***p<0.001, ****p<0.0001. See also Figure S5.

IL-5 is required for ICB-induced eosinophil accumulation and therapeutic benefit
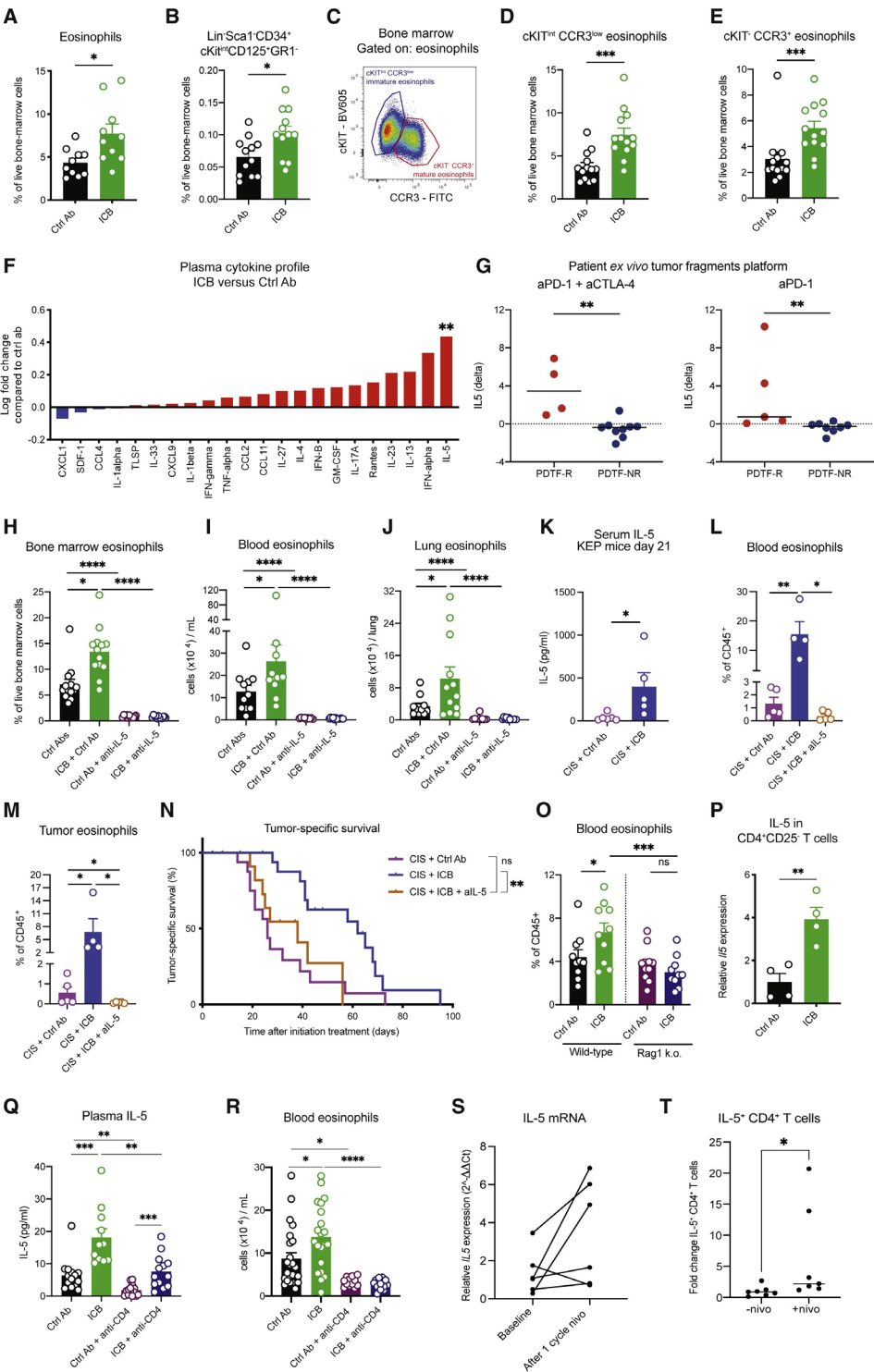
To investigate how ICB mediates the systemic eosinophil increase, we analyzed metastasis-bearing mice at different timepoints during the metastatic cascade and treatment. The eosinophil frequency in the blood increased after 7 days of ICB treatment and was maintained at high levels until at least 21 days (Figure S6A). Concomitantly, we observed an increase in eosinophils in the bone marrow (Figure 5A) and an increase of Lin⁻Sca1⁻ CD34+cKit^int CD125+Gr1⁻ cells, which have been previously described as eosinophil progenitors (Figure 5B & S6B)[43]. Furthermore, both immature (cKit^int CCR3^low) and fully mature (cKit⁻CCR3+) eosinophils increased in the bone marrow upon ICB (Figure 5C-E), while all other hematopoietic progenitor and immune cell populations remained unaffected (Figure S6C). Altogether, these observations suggest that the systemic increase of eosinophils induced by ICB is caused by increased eosinophil production in the bone marrow.

To assess which systemic factors induced by ICB could promote eosinophil production in the bone marrow, followed by systemic eosinophil accumulation, we measured the expression of a panel of cytokines in the plasma of metastatic mice. Strikingly, the only significantly increased cytokine upon ICB was IL-5 (Figure 5F & S6D), which is a major eosinophil regulator[44]. To investigate whether ICB treatment in human tumors induces IL-5 upregulation, we made use of the patient-derived tumor fragment (PDTF) platform[45]. This platform allows interrogation of the early immunological response of human tumor tissues upon *ex vivo* ICB treatment (aPD1 and combined aPD1+aCTLA4). Importantly, the observed *ex vivo* response (defined as previously described[45,46]) correlates with the clinical response of the patient[45]. We assessed the protein levels of IL-5 upon *ex vivo* ICB stimulation in tumors of patients with different tumor types. We observed an increase in IL-5 expression specifically in tumors that showed an immunological response to *ex vivo* ICB (PDTF-R) as compared to non-responding tumors (PDTF-NR), both upon aPD1 alone and combined aPD1+aCTLA4 treatment (Figure 5G & Table S4), demonstrating that IL-5 can be induced in human tumors by ICB.

To assess whether IL-5 drives eosinophil expansion upon ICB in metastasis-bearing mice, we blocked IL-5 using a neutralizing antibody. Indeed, the number of eosinophils in bone marrow, blood, and (pre-)metastatic lungs was drastically reduced (Figure 5H-J). Importantly, ICB did not promote an eosinophil increase after IL-5 blockade in any of the organs analyzed, indicating that ICB-induced eosinophils are IL-5 dependent. In line with

our observations in metastasis-bearing mice, serum IL-5 levels were similarly increased in tumor-bearing KEP mice during the responsive phase of CIS+ICB therapy (Figure 5K). IL-5 blockade during CIS+ICB therapy in KEP mice reduced eosinophil levels both systemically and intratumorally (Figure 5L,M), without affecting other myeloid cells (Figure S6E,F). Importantly, anti-IL-5 treatment abolished the therapeutic benefit induced by CIS+ICB (Figure 5N), phenocopying the effect of anti-SiglecF-induced eosinophil depletion (Figure 4D). Collectively, these findings demonstrate that IL-5 is a key driver of eosinophil accumulation and therapeutic benefit of CIS+ICB therapy.

Figure 5. CD4+ T cell-derived IL-5 is required for ICB-induced eosinophil expansion and therapeutic benefit. *(A-E) KEP metastasis-bearing mice were treated as indicated (Ctrl Ab, n=10-13; ICB, n=10-13) and sacrificed 10 days after start of treatment. Frequency of total eosinophils (Live Lin-CD127-CD11b+CD115-SiglecF+) (A), Live Lin-Sca1-CD34+cKit^int CD125+Gr1- eosinophil progenitors (B), representative dot plot (C) and quantification of cKit^int CCR3^low (D) and cKit-CCR3+ (E) eosinophils in bone marrow as determined by flow cytometry. (F) Relative expression of the indicated cytokines in the plasma of mice treated as described above (Ctrl Ab n=9, ICB n=10), determined by LEGENDplex, and normalized to Ctrl Ab-treated mice. (G) Fold change in IL-5 secretion by PDTF treated ex vivo with aPD-1+aCTLA-4 (left) or aPD-1 (right) compared to untreated condition, measured by LEGENDplex, comparing PDTF-R (responders) and PDTF-NR (non-responders), defined as described previously[45,46]. Tumor samples were collected from surgical material of patients with various tumor types (see STAR Methods and Table S4). (H-J) Metastasis-bearing mice were treated with IgG2a and IgG1 control antibodies (Ctrl Abs, n=14), ICB+IgG1 (n=14), IgG2a+anti-IL-5 (n=11) or ICB+anti-IL-5 (n=12) and analyzed 10 days after start of treatment. Number of eosinophils in bone marrow (H), blood (I) and lungs (J) determined by flow cytometry. Lung eosinophils were defined as CD45+CD11b+Ly6G-SiglecF+F4/80^int. (K) IL-5 levels in serum of tumor-bearing KEP mice analyzed 21 days after start of indicated treatments measured by ELISA. (L-M) Frequency of eosinophils in the blood (L) and tumor (M) of KEP mice treated as indicated and analyzed at tumor-related endpoint as determined by flow cytometry (n=4-5). Data from CIS+Ctrl Ab and CIS+ICB are the same mice as in Figure 3G. (N) Kaplan-Meier survival curves of KEP mice treated as indicated (CIS+Ctrl Ab, same curve as in Figure 3C; CIS+ICB, same curve as in Figure 3C; CIS+ICB+anti-IL-5, n=12, 3 censored). Log-rank (Mantel-Cox) test. (O) Number of eosinophils in blood of wild-type (wt) or Rag1 k.o. mice with KEP-derived orthotopic mammary tumors, treated as indicated (Ctrl Ab, wt n=10, Rag1 k.o. n=10; ICB, wt=10, Rag1 k.o. n=10), analyzed by flow cytometry when tumors reached an area of 144 mm². (P) IL5 gene expression in CD4+CD25- T cells sorted from blood of metastasis-bearing mice treated indicated (Ctrl Ab n=4, ICB n=4), determined by RT-qPCR. Relative expression to Ctrl Ab-treated mice is shown. (Q-R) Metastasis-bearing mice were treated with isotype control antibodies (Ctrl Ab, n=13-25), ICB (n=13-21), Ctrl Ab+anti-CD4 (n=14) or ICB+anti-CD4 (n=13) and sacrificed 10 days after start of the treatment. (Q) Plasma IL-5 levels, measured by ELISA. (R) Number of eosinophils in the blood, as determined by flow cytometry. Pooled data of two independent experiments. (S) IL5 gene expression determined by RT-qPCR in CD4+ T cells sorted from PBMCs at baseline and after one cycle of nivolumab metastatic TNBC patients treated in the control arm of the TONIC trial (n=6). (T) Fold change in frequency of IL-5+ CD4+ T cells among total CD4+ T cells from TNBC patients (n=7) treated ex vivo with aPD1 compared to untreated condition, measured by intracellular flow cytometry. All data are mean ±S.E.M, statistical analysis by unpaired t-test or Mann-Whitney, unless differently indicated. ns, not significant, *p<0.05, **p<0.01, ***p<0.001, ****p<000.1. See also Figure S6 and Table S4.* ▶▶▶

IL-5 producing CD4+ T cells drive eosinophil production and systemic expansion upon ICB

IL-5 can be produced by various cell types, principally CD4+ T cells, type 2 innate lymphoid cells (ILC2) and other innate immune cells, such as mast cells and eosinophils[44]. To evaluate whether adaptive or innate immune cells are needed to induce eosinophils upon ICB, we treated KEP tumor-bearing wild-type and *Rag-1*-deficient mice, which lack mature B and T cells but retain ILC2s and myeloid cells, with ICB or control antibody. Importantly, ICB failed to induce an increase in eosinophils in tumor-bearing *Rag*-1-deficient mice (Figure 5O), indicating that adaptive immune cells trigger eosinophil expansion upon ICB. Based on these findings, we hypothesized that CD4+ T cells are the main source of IL-5 upon ICB, and thus cause eosinophilia. Indeed, we observed increased expression of *IL-5* mRNA in circulating CD4+CD25- T cells upon ICB in metastasis-bearing mice (Figure 5P). Depletion of CD4+ T cells reduced plasma IL-5 levels and the number of eosinophils in bone marrow and blood of metastasis-bearing mice (Figure 5Q,R & S6G), suggesting a role for CD4+ T cells in eosinophil homeostasis. Importantly, in the absence of CD4+ T cells, there was reduced induction of IL-5 by ICB (Figure 5Q). Notably, ICB treatment still induced a slight but significant increase of serum IL-5 in CD4+ T cell-depleted mice compared to controls (Figure 5Q & S6G) suggesting other sources of IL-5, such as ILC2s, mast cells and eosinophils may produce the residual IL-5. Importantly, in line with the reduced induction of IL-5 upon ICB in the absence of CD4+ T cells, systemic eosinophil numbers did not increase upon ICB in CD4+ T cell-depleted mice (Figure 5R & S6H). In addition to mature bone marrow eosinophils, the frequency of Lin-Sca1-CD34+cKit^IntCD125+Gr1- eosinophil progenitors did not increase upon ICB after CD4+ T cell depletion (Figure S6I). These data demonstrate that CD4+ T cells are required for the ICB-induced increase in systemic IL-5 levels, eosinophil production in the bone marrow and systemic eosinophil accumulation. Importantly, CD4+ T cell depletion also reduced the number of circulating eosinophils in metastasis-bearing mice treated with CIS+ICB (Figure S6J), confirming that CD4+ T cells are required for eosinophil increase not only upon ICB treatment alone, but also during CIS+ICB. To exclude the potential contribution of T_regs in ICB-induced eosinophilia, we used KEP tumor-bearing *Foxp3-DTR-GFP* mice allowing specific depletion of FOXP3 expressing T_regs (Figure S6K,L)[47]. Upon T_reg depletion, blood eosinophil numbers during ICB were further increased compared to T_reg-proficient mice (Figure S6M), indicating that T_regs do not facilitate ICB-induced eosinophil expansion, but hamper ICB-induced eosinophilia.

To address whether CD4+ T cells are a source of IL-5 in TNBC patients, we utilized peripheral blood mononuclear cells (PBMCs) isolated from patients of the TONIC trial treated with ICB without induction treatment at baseline and after one cycle of nivolumab and performed RT-qPCR for *IL-5* mRNA in sorted CD4+ T cells. 5 out of 6 patients had an increase in *IL-5* transcript in CD4+ T cells upon nivolumab treatment compared to baseline (Figure 5S). To further demonstrate that CD4+ T cells produce IL-5 protein in response to nivolumab, we stimulated PBMCs from TNBC patients with nivolumab for 48 hours and analyzed

intracellular IL-5 in CD4+ T cells by flow cytometry. These data show a statistically significant fold change in IL-5+ CD4+ T cells upon nivolumab stimulation (Figure 5T), demonstrating that aPD-1 induces IL-5 expression in circulating CD4+ T cells of TNBC patients. Collectively, our data demonstrate that IL-5 producing CD4+ T cells drive eosinophil expansion upon ICB.

IL-33 drives eosinophil recruitment to the TME and is required for the therapeutic benefit of CIS+ICB

Although ICB alone leads to systemic eosinophil accumulation, eosinophil recruitment to the tumor and their subsequent contribution to therapeutic benefit was only observed upon CIS+ICB combination therapy in our pre-clinical models (Figure 3). We therefore asked which eosinophil-recruiting or activating factors trigger the intratumoral accumulation of eosinophils upon CIS+ICB. Analysis of a broad panel of eosinophil-related cytokines and chemokines revealed that IL-33 was specifically increased upon CIS+ICB in the plasma of metastasis-bearing mice at the responsive phase of therapy (Figure 6A). Similarly, IL-33 levels were increased in tumor lysates and serum of KEP tumor-bearing mice treated with CIS+ICB (Figure 6B & S7A). Importantly, in patients with metastatic TNBC responding to ICB we observed a strong positive correlation between the eosinophil gene signature and *IL-33* expression in metastatic lesions which was not observed in non-responders, suggesting a link between *IL-33* expression and eosinophil infiltration in the TME (Figure 6C). Of note, in both patients and mice, cisplatin alone was not sufficient to induce a statistically significant increase in IL-33 levels (Figure 6B & S7A,B). IL-33 is an alarmin that amplifies immune responses during inflammation[48]. IL-33 directly promotes eosinophil activation, adhesion and survival[49][50], and IL-33 contributes to several eosinophilic disorders[51]. In the cancer context, IL-33 has been associated with both pro- and anti-tumor functions[14,52,53]. To assess the functional role of IL-33 in intratumoral eosinophil accumulation, we made use of the IL-33-TRAP fusion protein, a high-affinity IL-33 antagonist[54]. In line with our earlier observation that IL-5 is responsible for ICB-induced systemic eosinophilia (Figure 5), IL-33 neutralization did not affect systemic eosinophil accumulation during CIS+ICB (Figure 6D). However, intratumoral eosinophil infiltration was abrogated upon IL-33 blockade (Figure 6E), indicating that IL-33 is required, directly or indirectly, for eosinophil recruitment to the tumor. IL-33-TRAP also prevented the intratumoral CIS+ICB-induced CD8+ T cell activation without affecting other immune populations (Figure 6F & S7C,D), phenocopying the effect of eosinophil depletion (Figure 4). Importantly, IL-33-TRAP blocked the therapeutic benefit provided by CIS+ICB (Figure 6G). In summary, these data demonstrate that IL-33 is required for eosinophil infiltration in the tumor, CD8+ T cell activation, and therapeutic benefit observed upon ICS+ICB. These preclinical findings are supported by our clinical observation that increased intratumoral eosinophil infiltration is strongly correlated to IL-33 expression as well as to CD8+ T cells in the TME of TNBC patients responding to ICB (Figure 2C-H & 6C).
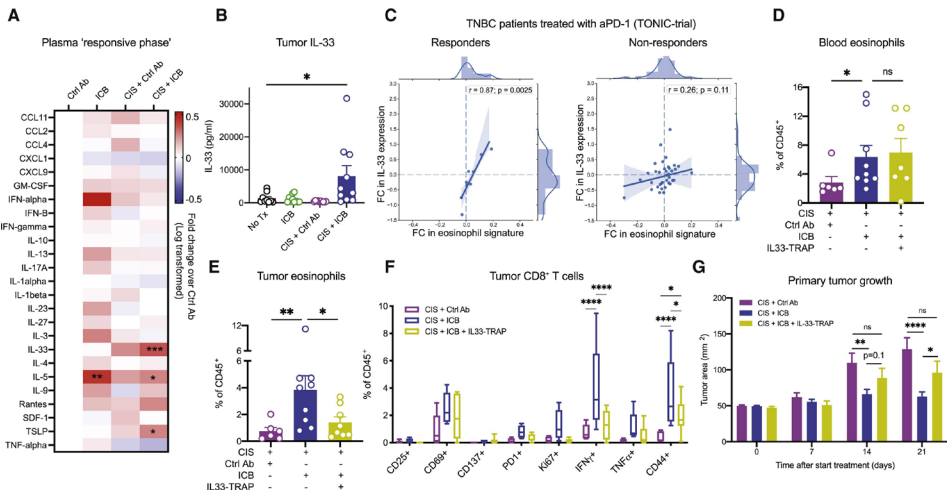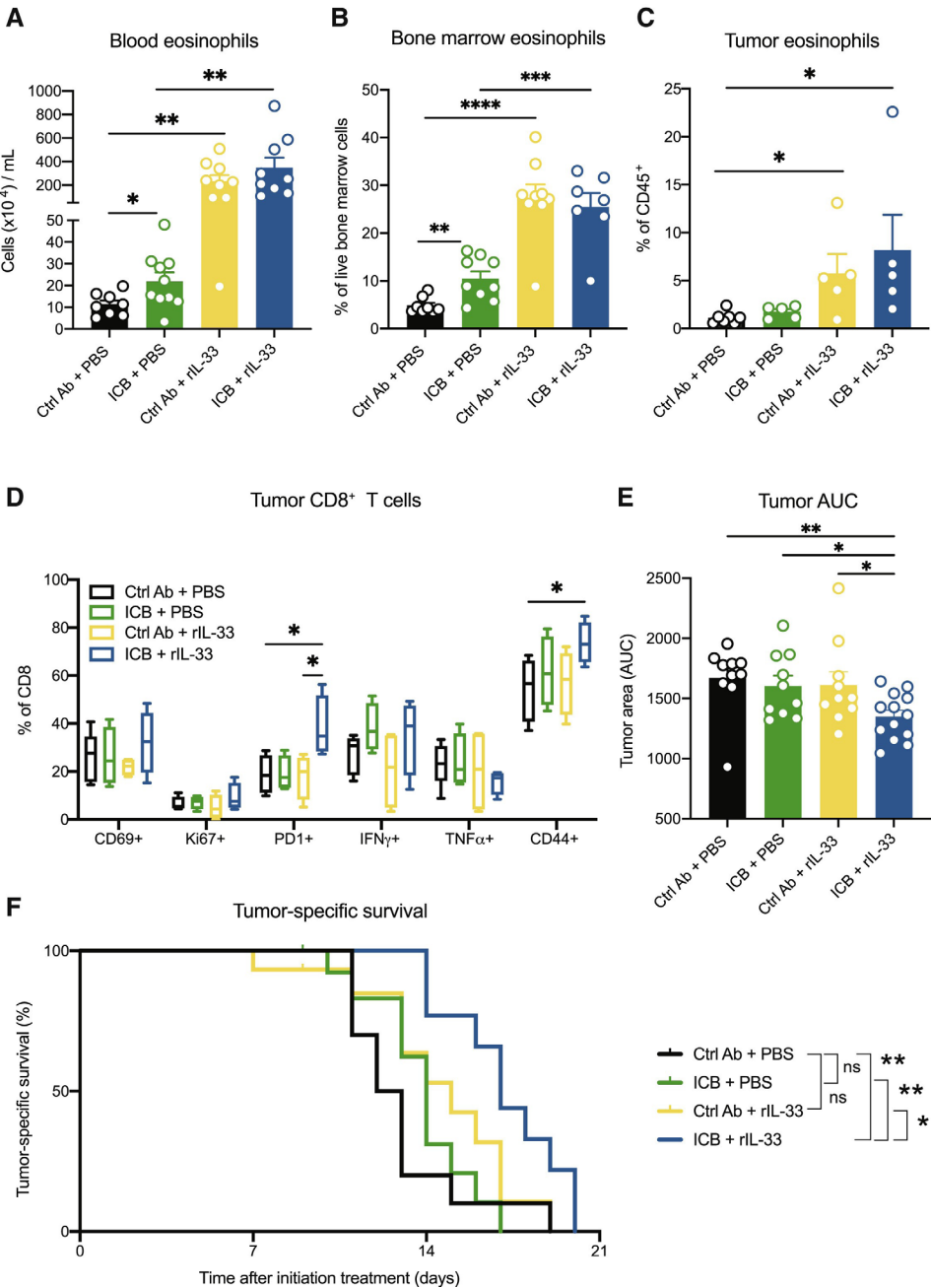
7

Figure 6. IL-33 drives intratumoral eosinophil infiltration and is required for the therapeutic benefit of CIS+ICB. *(A) Relative expression of the indicated cytokines in plasma of metastasis-bearing mice treated as described before (Ctrl Ab n=9 (same data as in Figure 5F), ICB n=10 (same data as in Figure 5F), CIS+Ctrl Ab n=9, CIS+ICB n=13), determined by LEGENDplex. Data is normalized to Ctrl Ab-treated mice. 1-way ANOVA or Kruskal-Wallis followed by Dunnett's or Dunn's multiple comparisons test, comparing each treatment against control-treated mice, for each cytokine. (B) IL-33 levels in tumor lysates of end-stage tumors as determined by LEGENDplex (n=9-10). 1-way ANOVA followed by Dunnett's multiple comparisons test, comparing each group against untreated. (C) Correlation between the fold change (baseline to on-nivolumab) in eosinophil gene signature (described in Figure 2B) and the fold change (baseline to on-nivolumab) in IL33 in RNA-seq analysis of paired biopsies from responding (left) and non-responding (right) patients with metastatic TNBC. Graph characteristics as in Figure 2. (D-E) Frequency of eosinophils in the circulation (D) and tumor (E) of KEP mice analyzed 21 days after start of treatment determined by flow cytometry (n=6-9). Mean ±S.E.M., Mann-Whitney. (F) Frequency of indicated activation markers expressed on intratumoral CD8+ T cells, determined by flow cytometry (n=5-9). Data from CIS+Ctrl Ab and CIS+ICB are same mice as Figure 4G. Boxes represent median and interquartile range; whiskers full range. 2-way ANOVA followed by Tukey's multiple comparison test. (G) Average tumor growth size ±S.E.M. of KEP mice treated as indicated (CIS+Ctrl Ab n = 23, CIS+ICB n=32), CIS+ICB+IL33-TRAP n = 12). Unpaired t-test. ns, not significant, *p<0.05, **p<0.01, ***p<0.001, ****p<000.1. See also Figure S7A-D.*

Figure 7. Recombinant IL-33 therapy engages eosinophils and enhances ICB response . *(A-C) Mice bearing orthotopically transplanted KEP tumors were treated as indicated (Ctrl Ab+PBS, n=10; ICB+PBS, n=15; Ctrl Ab+rIL-33, n=15; ICB+rIL-33, n=15). Frequency of eosinophils in the circulation (A), bone marrow (B), and tumor (C) were analyzed in the responsive phase of therapy, determined by flow cytometry. Mean ±S.E.M., t-test. (D) Frequency of indicated activation markers expressed on intratumoral CD8+ T cells in responsive phase of therapy, determined by flow cytometry (n=5-7). Boxes represent median and interquartile range; whiskers full range. 2-way ANOVA followed by Tukey's multiple comparison test. (E) Area under curve (AUC) of growth curves was determined up to day 14 after start of treatment. Mean ±S.E.M., 1-way ANOVA. (F) Kaplan-Meier survival curves showing tumor-related survival. Log-rank (Mantel-Cox) test. ns, not significant, *p<0.05, **p<0.01, ***p<0.001, ****p<0.0001. See also Figure S7E-F.* ▶▶▶

Recombinant IL-33 engages eosinophils and enhances response to ICB

In light of our finding that IL-33 drives eosinophil infiltration into the tumor, we hypothesized that deliberate induction of intratumoral accumulation of ICB-educated eosinophils by recombinant IL-33 (rIL-33) might represent a viable strategy to enhance the therapeutic benefit of ICB in breast cancer, in absence of chemotherapy. Treatment of mice bearing orthotopically transplanted KEP tumors with rIL-33 alone or in combination with ICB resulted in increased eosinophils in the blood and bone marrow, as well as increased intratumoral eosinophil infiltration (Figure 7A-C). However, only the combination of ICB and rIL-33 increased CD8+ T cell activation, and most notably increased the frequency of effector CD44+ and PD-1+ CD8+ T cells (Figure 7D), without altering other immune populations (Figure S7E-F). Importantly, IL-33-mediated engagement of eosinophils during ICB and the resulting CD8+ T cell activation was accompanied by improved tumor control and extension of survival (Figure 7E-F). Collectively, these data provide proof-of-principle that rIL-33 can engage eosinophils and represents a viable strategy to enhance response to ICB in breast cancer.

Discussion

In this study, we take a translational approach by combining longitudinal analysis of fresh blood and tumor biopsy samples of a patient cohort with functional experiments in clinically relevant mouse models to identify the IL-5 and IL-33-eosinophil axis as crucial mediator of ICB response in breast cancer. The effect of ICB on myeloid cells and the influence of myeloid cells on ICB response is often overlooked. We here show that an ICB-induced increase in systemic IL-5, driven by CD4+ T cells, pushes myelopoiesis towards increased eosinophil production resulting in systemic eosinophil accumulation. Here, parallels can be drawn with allergic conditions in which CD4+ T cells and eosinophils have a pathogenic function. In patients with allergic asthma, CD4+ T cells play a major role in the pathophysiology driving eosinophil expansion via IL-5 production[44,55]. How ICB triggers this mechanism in the cancer context is not fully elucidated, but we demonstrated that CD4+ T cells of TNBC patients upregulate IL-5 *in vivo* and *in vitro* upon stimulation with nivolumab/aPD-1, indicating that ICB can directly stimulate CD4+ T cells to secrete IL-5. A role for PD-1/PD-L1 signaling in controlling IL-5 secretion from CD4+ T cells has previously been proposed in the context of allergy, where *in vitro* exposure of human allergen-specific CD4+ T cells to PD-1 blockade stimulated their production of IL-5, among other cytokines[56]. Altogether, we demonstrate that ICB-activated CD4+ T cells use a similar mechanism via IL-5 to drive eosinophil accumulation in cancer patients and preclinical models.

Although neutrophils and basophils also derive from common-myeloid progenitors (CMP), express IL5R and can respond to IL-5 in certain inflammatory conditions[57,58], IL-5 is the central cytokine specific to eosinophil development in the bone marrow[59]. IL-33 is also implicated in eosinophil development, capable of inducing IL-5 and upregulating IL-5Rα on eosinophil progenitors[60]. Interestingly, we observe that ICB, in absence of chemotherapy, increases IL-5 expression but not IL-33, indicating that ICB-induced IL-5 is not dependent on IL-33. This is further supported by our observation that systemic eosinophil abundance was unchanged upon IL-33 blockade during CIS+ICB, confirming that IL-5 is the main driver of eosinophil production in the bone marrow and systemic eosinophil accumulation upon ICB.

We demonstrate that ICB can be sufficient to induce systemic eosinophil increase, but in the majority of patients and in our mouse models (which do not respond to ICB alone), this is not enough to achieve intratumoral eosinophil infiltration. We uncover that induction of IL-33 is needed to overcome this threshold and enable eosinophil infiltration into the tumor. IL-33 can either directly affect eosinophil activation and recruitment, as has been shown for eosinophils in inflammatory diseases[49,50], or indirectly by acting on other cells of the tumor microenvironment, for instance by promoting chemokine expression in tumor cells[16]. IL-33 can be passively released by epithelial cells upon cellular damage[61] or actively secreted by immune cells during infection[62] and tumor cells themselves[63]. Importantly, in our mouse models cisplatin alone was not sufficient to increase IL-33 expression, indicating that cell damage induced by chemotherapy is not the sole driver of increased IL-33. By combining CIS+ICB we were able overcome this threshold and kick start the IL-33 aspect of the cascade in our mouse models. Future research is warranted to understand which other therapeutic modalities besides cisplatin may induce intratumoral IL-33 and whether these depend on cancer cell-intrinsic features or context-dependent mechanisms remains to be elucidated. For example, in patients the net-biological effect of IL-33 is influenced by levels of soluble ST2 (also known as *IL1RL1*), which acts as a decoy receptor for IL-33, and for which different genetic variants exist in humans[64]. Thus, adding layers of complexity to the regulation of the identified immune axis.

Identifying the source of IL-33 and deciphering how its production is regulated during ICB would be important to further harness its full therapeutic potential to synergize with ICB.

The synergy between rIL-33 and ICB has been studied in highly immunogenic models[65,66], but not, to our knowledge, in poorly immunogenic breast cancer models. Our observation that IL-33 expression correlates with an eosinophil signature in metastases of breast cancer patients that respond to ICB and our preclinical proof-of-principle study demonstrating that rIL-33 mobilizes eosinophils to improve ICB response, indicate that IL-33 represents an attractive engager of eosinophils in breast cancer patients during ICB. However, IL-33 is reported to have pleiotropic functions[67]. The systemic administration of rIL-33, as performed in this study, induced an effective but modest anti-tumor response, especially in comparison with CIS+ICB, likely because of the direct anti-tumor effect and additional immunomodulatory properties of cisplatin[68,69]. Further studies are needed to evaluate whether IL-33 in

combination with ICB could be used to specifically engage eosinophils in patients, for instance by local IL-33 administration, although, in the context of multi-organ metastatic disease, local administration of rIL-33 would be challenging.

It has been suggested that ICB-induced eosinophils may exert direct tumoricidal effects or enhance anti-tumor immunity by changing the tumor vasculature or reshaping the immune landscape[6]. Eosinophils can facilitate recruitment of CD8+ T cells by expression of T cell chemoattractants[11,25] or promote T cell activation in the tumor[13]. We demonstrate that eosinophils enhance CD8+ T cell activation, rather than their recruitment, in mammary tumors responding to CIS+ICB. In line with our findings in mouse models, we observed that increased expression of an eosinophil gene signature correlated with increased CD8+ T cell and IFNγ gene signatures in metastatic lesions of breast cancer patients responding to ICB. This suggests that in TNBC patients, eosinophils also contribute to ICB response via activation of CD8+ T cells, as was previously proposed for melanoma patients[19]. It remains to be determined whether eosinophils exert this function directly, for example by producing T cell stimulating cytokines or chemokines, or indirectly via activation of for instance dendritic cells, as has been described during allergic inflammation[70-72].

In our study, the treatment of mice and patients differed. In our mouse models, cisplatin and dual ICB was needed to induce responses, while patients were treated with ICB alone or preluded by a brief induction treatment. Despite these differences in dosage regime and type of ICB therapy, we strikingly uncovered the same phenomena of increased eosinophils in response to ICB, indicating that the mechanism described in this study is a general feature of effective ICB response. This is supported by our observation that response to ICB leads to eosinophil accumulation in several cancer types and by a recent small series of 14 TNBC patients in which an eosinophil increase was observed upon response to anti-PD-L1 and paclitaxel[73]. Additionally, we validated in patients the different elements of the mechanism identified in our preclinical models. We observed that circulating CD4+ T cells of TNBC patients upregulate IL-5 expression upon nivolumab treatment *in vivo* and *in vitro*. Moreover, our data demonstrating that IL-5 is secreted in tumors that show an immunological response upon *ex vivo* ICB stimulation with either aPD-1 or combined aPD-1+aCTLA-4, further strengthen our conclusion that IL-5 induction is a common mechanism across different tumor types and ICB regimens with or without chemotherapy.

Finally, it has been suggested that increased eosinophil counts upon ICB could be used as an early predictive biomarker for response[19-24]. Although we see expansion of these cells upon response to ICB in patients with metastatic TNBC, NSCLC and early-stage pMMR CC, on-treatment response biomarkers are rarely used in oncology due to widely available imaging methods for response assessment. Moreover, eosinophil expansion was not restricted to responders, but was also observed in a proportion of non-responders as previously reported, limiting its potential for clinical decision making[19-24]. Therefore, increased

eosinophils upon ICB response, combined with our preclinical proof of their causal role in ICB response, should be considered as an important lead for the development of novel immunomodulatory strategies to engage eosinophils rather than a biomarker.

In conclusion, this study highlights that combining translational research on clinical trials with mechanistic research in preclinical models is a powerful strategy to unravel novel mechanisms of ICB response. Our findings emphasize that successful anti-tumor immune responses are not only reliant on T cells, but that crosstalk with myeloid cells is critical for an effective response to ICB, providing new avenues for future research in immuno-oncology.

7

STAR Methods

RESOURCE AVAILABILITY

Lead contact
Requests for further information and resources of this study should be directed to Karin de Visser (k.d.visser@nki.nl)

Materials availability
This study did not generate new unique reagents.

Data and code availability
- RNA-sequencing data on mouse eosinophils generated in this study has been deposited at Gene Expression Omnibus (GEO) under accession number GSE210895 and are publicly available from the date of publication. RNA-sequencing data on tumor biopsies of TNBC patients treated in the TONIC-trial stage 1 are deposited at the European Genome-phenome Archive (EGA) under accession number EGAS0001003535 and will be made available from the corresponding author on reasonable request. NanoString data from TONIC-trial stage 1 and RNAseq data of TNBC patients treated in TONIC-trial stage 2 reported in the paper are not deposited in a public repository pending ongoing work but can be made available from the corresponding authors upon reasonable request. All human data requests will be reviewed by the Institutional Review Board (IRB) of the NKI and applying researchers have to sign a data transfer agreement after IRB approval before the data can be released.
- This paper does not report original code.
- Any additional information required to re-analyze the data reported in this paper is available from the lead contact upon request.

EXPERIMENTAL MODEL AND SUBJECT DETAILS
Preclinical models
The transgenic *Keratin14-cre;Cdh1*[F/F]*;Trp53*[F/F] (KEP) model for primary mammary tumorigenesis [34] (FVB/N genetic background), KEP-based orthotopic mammary tumor model and the KEP-based model for spontaneous breast cancer metastasis [35] were used as previously described [26,27]. Female KEP mice were monitored twice per week for spontaneous tumor formation by palpation starting at the age of 3.5 months. KEP mice develop palpable tumors between 6-8 months of age[34]. The perpendicular diameters of the tumors were measured using a caliper and tumor area was calculated accordingly. Female FVB/N mice of 8-12 weeks of age were obtained from Janvier Labs. *Rag1* k.o. in FVB/N genetic background were a gift from L. Coussens[74]. *Cdh1*[F/F]*;Trp53*[F/F]*;Foxp3*[DTR-GFP] mice[75] in FVB background were generated by the

Animal Modeling Facility (AMF) of the Netherlands Cancer Institute. All mice were kept in individually ventilated cages at the animal laboratory facility of the NKI. Food and water were provided ad libitum. All animal experiments were approved by the Animal Ethics Committee of the NKI and performed in compliance with the national and European guidelines for animal care and use.

Clinical trial procedures
Trial procedures were performed as described previously in the respective publications [28-31]. All patients included in stage 1 [28] and stage 2 of the TONIC-trial (NCT02499367) were included in the current analysis. In stage 1, 70 patients were included in the TONIC-trial, of which 67 patients received nivolumab and were available for efficacy and translational analysis, as previously described [28]. An additional 47 patients were included in stage 2 of the trial, of which 44 patients received nivolumab and were available for efficacy and translational analysis. From these 111 patients (Table S1), paired flow cytometry on fresh blood (baseline, after two-week induction period and after 3 cycles of nivolumab) was performed on 55 patients and paired routine eosinophil counts were available for 90 patients (sample availability in Table S2 and Figure S1b). Progression-free survival was measured as time between date of randomization and date of progression according to iRECIST or date of death. Overall survival was measured as time between first date of nivolumab and date of last follow-up or date of death. Data was cut-off at 1 March 2021.

Patients with metastatic NSCLC were treated in the PEMBRO-RT trial (NCT02492568)[29] at the NKI (paired data for n=40 from the total of 55 patients treated at the NKI and the total of 76 patients included in the trial), in which patients were randomized to pembrolizumab with or without upfront radiation [29]. To investigate eosinophil dynamics in patients with metastatic dMMR tumors, we made use of patients treated with nivolumab in the NKI within the dMMR cohort (paired data for n=9 of the total 11 patients treated at the NKI and the total of 30 patients included in the cohort) of the DRUP-trial (NCT02925234) [31]. Finally, patients with early-stage colon cancer (either dMMR (n=21) or pMMR (n=17)) were treated in the NICHE-trial, in which patients are treated with neo-adjuvant ipilimumab (1mg/kg) and nivolumab (3mg/kg), with or without additional celecoxib in pMMR patients (NCT03026140)[30]. In the patients with metastatic disease, response was defined as complete response (CR), partial response (PR) and stable disease (SD) of at least 24 weeks, defined according to RECIST1.1 [76]. Best overall response in the TONIC-trial was measured according to iRECIST[77]. Response in the NICHE-trial was defined as any pathological response (>10% tumor regression), assessed on surgical material after neo-adjuvant treatment. All clinical study protocols were approved by the medical-ethical committee of the NKI and conducted in accordance with the ICH Harmonized Tripartite Guideline for Good Clinical Practice and the principles of the Declaration of Helsinki. All patients provided written informed consent to participate in the clinical trial.

METHOD DETAILS

Preclinical intervention studies

In the spontaneous KEP model, all treatments started when tumor area reached 50mm^2. For the KEP-based orthotopic mammary tumor model, mammary tumor pieces of 1mm^2 size derived from KEP mice were orthotopically transplanted into the mammary glands of female FVB/N mice. In this model, treatments started when tumor area reached 25 mm^2. For the survival experiments and endpoint analysis mice were sacrificed when the cumulative tumor burden reached 225mm^2. KEP mice were sacrificed 21 days after initiation treatment to analyze the 'responsive phase' or at a tumor size of 150mm^2 for the KEP-based orthotopic mammary tumor model. Cisplatin (Accord Healthcare Limited) was injected intravenously once every two weeks at 5mg/kg, for a maximum of 4 cycles. Anti-mouse PD-1 (RMP1-14, BioXCell), anti-mouse CTLA-4 (9D9, BioXCell) or control (2A3, BioXCell) antibodies were each given intraperitoneally at 100µg per mouse, twice per week. Anti-CD8 (2.43, BioXCell) or anti-CD4 (GK1.5, BioXCell) antibody were given intraperitoneally at 200µg per mouse, twice per week. Anti-mouse SiglecF (238047, R&D systems) and control antibody (2A3, BioXCell) were administered intraperitoneally at 20µg per mouse, three times a week. Anti-IL-5 (TRFK5, BioXCell) and control antibody (HRPN, BioXCell) were given intraperitoneally at 500µg per mouse, twice per week. Recombinant mouse IL-33 (Biolegend) was given intraperitoneally at 0,4 µg per mouse, three times a week. IL-33-TRAP (provided by Rudi Beyaert laboratory, VIB, Belgium) was given intraperitoneally at 50µg per mouse daily. For the T$_{reg}$ depletion in *Foxp3-GFP-DTR* mice, DT (Diptheria toxin from *Corynebacterium diphteriae*) was given intraperitoneally at 25µg/kg, at day 0 and day 4 after start of treatment. All antibody treatments continued until the experimental endpoint was reached.

For metastasis experiments, mammary tumor pieces of 1mm^2 size derived from KEP mice were orthotopically transplanted into the mammary glands. Mammary tumors were surgically removed when they reached the size of 100mm^2. In the metastasis experiments, all treatments started 15 days after mastectomy, when all mice have established metastasis in the lung and/or lymph node, and treatments continued until the experimental endpoint. All treatments were performed as described above. For survival experiments, mice were sacrificed when they developed signs of distress caused by metastatic disease (respiratory distress) or when lymph node metastasis reached the size of 225mm^2. For analysis of 'responsive phase', metastasis-bearing mice were sacrificed 10 days after start of treatment for Ctrl Ab and ICB groups and 21 days for CIS+Ctrl Ab and CIS+ICB groups.

Flow cytometry analysis

Tumors and organs from KEP mice and FVB/N mice with metastatic breast cancer were collected in ice-cold PBS. Blood was withdrawn by tail vein or heart puncture and collected in K$_2$EDTA-containing tubes (BD Microtainer Blood Collection Tubes). Tumor tissues and lungs were mechanically minced using the McIlwain tissue chopper (Mickle Laboratory Engineering) and enzymatically digested at 37°C in DMEM medium containing 3mg/ml collagenase type A (Roche) plus 25µg/ml of DNase I (Sigma) for 45 min or in 100µg/mL Liberase TM (Roche) for 30 min, respectively. Half of the lymph nodes and spleen were enzymatically digested in RPMI medium containing 3mg/ml collagenase type IV (ThermoFisher Scientific), 2mM CaCl$_2$, 2% FCS and 25µg/mL DNase I for 30 min at 37°C and used to stain for myeloid cell populations. The other half was directly processed into single cell suspensions and used for lymphoid cell panels. All digestion reactions were stopped by adding cold DMEM medium containing 10% FCS. For the analysis of bone marrow, tibia and femurs were flushed with PBS and processed as the other organs. Single-cell suspensions were obtained by mashing through 70µm filter and resuspended in PBS containing 0.5% BSA (Roche) and 2mM EDTA (Lonza). Blood, spleen, lungs and bone marrow samples were treated for 5 min at room temperature with NH$_4$ lysis buffer to remove erythrocytes.

For flow cytometry analysis of patient sample preparations, peripheral blood was collected in an K$_2$EDTA vacutainer (BD) and processed and analyzed within 24 hours. Red blood cells were lysed (lysis buffer: dH$_2$O, NH$_4$Cl, NaHCCO$_3$, EDTA) and cells were resuspended in PBS containing 0.5% BSA and 2mM EDTA. To obtain absolute white blood cell counts per mL of human blood, the total post-lysis cell count was obtained using the NucleoCounter NC-200 (Chemometec) Automated cell counter was divided by the total volume (mL) of blood.

For intracellular cytokine staining, cells were stimulated *ex vivo* with 50ng/ml PMA, 1µM ionomycin and Golgi-Plug (1:1000; BD) for 3h at 37°C in IMDM medium supplemented with 8% FCS, 100 IU/ml Penicillin-Streptomycin (Roche) and 0.5% β-mercaptoethanol. For surface antigen staining, cells were first incubated with rat anti-mouse CD16/CD32 antibody (1:100; Mouse Fc Block, BD Bioscience) or human FcR Blocking Reagent (1:100 Miltenyi) for 15 min at 4°C and then incubated with fluorochrome-conjugated antibodies for 30 min at 4°C, in the dark. For intracellular antigen staining, cells were fixed with Fixation/Permeabilization solution 1X (Foxp3/Transcription Factor Staining Buffer Set, eBioscience) for 30 min at 4°C and stained with fluorochrome-conjugated antibodies in Permeabilization buffer 1X (eBioscience) for 30 min at room temperature. Viability was assessed by staining with either 7AAD staining solution (1:20; eBioscience), Zombie Red Fixable Viability Kit (1:800 BioLegend) or with Fixable Viability Dye APC-eFluor780 (1:1000; eBioscience). Data acquisition was performed on BD LSRII flow cytometer using Diva software (BD Biosciences) and data analysis was performed using FlowJo software version 10.6.2. All used flow cytometry antibodies can be found in Key Resources Table. Gating strategies are displayed in Figure S8 & 9.

Immunohistochemistry

KEP tumors were fixed for 24h in 10% neutral buffered formalin, embedded in paraffin and sectioned at 4µm. CD4, CD8, FOXP3 and Ly6G stainings were performed by the Experimental

Animal Pathology facility of the NKI. Antibodies are listed in Key Resources Table. For MBP staining, sections were deparaffinized in xylene for 20 min, rehydrated, and incubated with 3% H_2O_2 for 10 min at room temperature. Antigen retrieval was performed using Pepsin solution (ThermoFischer Scientific) for 10 min at room temperature. As blocking solution PBS with 2.5% BSA and 10% normal goat serum was used for 30 min at room temperature. Sections were incubated with rat anti-mouse MBP antibody (1:350, clone MT-14.7.3, Lee Laboratory, Mayo Clinic) diluted in 0.5X blocking solution, overnight at 4°C. Biotinylated goat anti-rat IgG antibody (1:300, Southern Biotech) was used as secondary antibody. Streptavidin-HRP and DAB solution (DAKO) were used following manufacturer's instructions. Sections were counterstained with hematoxylin solution. Slides were scanned using Aperio ScanScope and analyzed with Aperio ImageScope software version 12.4.3 (Aperio, Vista).

RNA-sequencing of mouse eosinophils

For the transcriptomic analysis, a minimum of 35000 eosinophils (CD11b$^+$ Ly6G^{low} SSC^{high} F4/80$^+$) were sorted from the blood in RLT buffer containing 1% β-ME, using a BD FACSAria™ Fusion Cell Sorter. RNA was isolated following RNeasy Mini Kit (Qiagen) protocol, using 80% ethanol instead of RPE buffer. Smart-seq2 library preparation was performed as previously described[78], using 2100 Bioanalyzer System (Agilent) for quality control. Only samples with RIN ≥ 7 were used for RNA-sequencing analysis. The strand-specific reads (65bp single-end) were sequenced with the HiSeq 2500 System (Illumina). Demultiplexing of the reads was performed with Illumina's bcl2fastq software and demultiplexed reads were aligned against the mouse reference genome (build 38) using HISAT2. HISAT2 was supplied with known set of gene models (Ensembl version 87). Qlucore Omics Explorer (Qlucore AB, Lund, Sweden) software was used to calculate and visualize differentially expressed genes (p<0,05) and sample variation, after having discarded genes with fewer then 30 mapped reads in at least 9 samples and performed data normalization by TMM method. Gene set enrichment analysis (GSEA) was performed using the GSEA program version 4.0.3 (Broad Institute). Hallmarks gene sets from Molecular Signatures Database v7.2 were used. Mouse gene symbols were remapped to human orthologues using Mouse_Gene_Symbol_Remapping_Human_Orthologs_MSigDB.v7.2.chip annotation file.

Cytokine analysis

For the analysis of cytokines and chemokines expression in mouse plasma, serum or tumor lysate, custom-made Legend Plex bead-based immunoassay (Biolegend) was used, according to manufacturer instructions. 50 µg of total protein from lysed tissues was used for measurements. Data acquisition was performed on LSRFortessa (BD Biosciences) flow cytometer using Diva software (BD Biosciences) and analyzed using LEGENDplex™ Data Analysis Software Suite (Biolegend). In addition, mouse IL-5 ELISA detection kit (BioLegend) was used, according to manufacturer instructions.

Routine eosinophil counts in patient cohorts

Eosinophil counts were measured with a XN-2000 Hematology Analyzer of Sysmex at the diagnostic Clinical Chemistry Department. The variation coefficient was below 10%.

RNA extraction and NanoString gene expression analysis

RNA was isolated from freshly frozen sections of biopsies as previously described [28]. For each patient, sequential biopsies were taken from the same metastatic lesion, however per patient, the site of the metastatic lesion was different (predominantly, but not only, lymph nodes, recurrent lesion in breast, liver, skin). mRNA expression was measured with the nCounter technology provided by NanoString Technologies as previously described [28]. NanoString mRNA counts were available for patients included in stage 1 of the TONIC-trial (paired metastatic biopsies pre-nivolumab and on-nivolumab n = 26).

RNA-sequencing on patient tumor biopsies

The RNA-sequencing data was aligned to the reference genome GRCh38 with STAR (version 2.7.1a) [79] with two-pass mode option set to "Basic". For comparison between patients, a median of ratios normalization was performed with Deseq2 R package (version 1.24.0, [80]) and for within-patient comparisons TPM normalization was used. Data was analyzed using Python 3.7.6, with pandas (version 1.0.1,[81,82]) and NumPy (version 1.18.1,[83] packages. Plots were created using Matplotlib (version 3.1.3, [84]) and Seaborn (version 0.10.0,[85]), statistical annotation was added using statannot (version 0.2.2,[86]). All gene-signatures are listed in Table S3. Mean normalized expression values of individual genes were taken as a signature score. A fold change of the signature score baseline vs. on-nivolumab was taken for each signature. RNA-sequencing on paired metastatic lesions (baseline and on-nivolumab) was available for 48 patients, included in both stages of the trial.

RT-qPCR

Human CD3$^+$ CD4$^+$ T cells were sorted from TONIC patient PBMCs into RLT buffer containing 1% β-ME, using a BD FACSAria™ Fusion Cell Sorter. RNA was isolated following RNeasy Micro Kit (Qiagen) protocol. RNA was converted to cDNA with an AMV reverse transcriptase using Oligo(dT) primers (Invitrogen). For mouse CD4$^+$CD25$^-$ T cells, RNA was converted to cDNA using High-capacity cDNA reverse transcription kit (ThermoFisher Scientific), following kit instructions. cDNA (20 ng per well) was analyzed by SYBR green real-time PCR with 500 nM primers using a LightCycler 480 thermocycler (Roche). *Gapdh* was used as a reference gene. Primer sequences used for each gene are listed in the Key Resources Table. Fold change in expression was calculated using $2^{-(\Delta Ct.x - average(\Delta Ct.control))}$.

7

Human PBMC stimulation

PBMCs were isolated at baseline from patients with metastatic TNBC in the control arm of the TONIC trial. Patient PBMCs were seeded at a density of 500,000 cells per well in 96-well plates in DMEM (Sigma), 10% FBS (Sigma), 1 mM sodium pyruvate (Sigma), 1x MEM nonessential amino acids (Sigma), 1x Glutamax, 100 ng/ml penicillin/streptomycin, 50 nM 2-mercaptoethanol (Sigma). Cells were stimulated with a suboptimal concentration of 0.5µg/ml plate bound anti-CD3 (OKT3, BioLegend) and 2µg/ml anti-CD28 (28.2, eBioscience) for 48 hours. Anti-PD1 (Nivolumab,10µg/ml) was added where indicated. GolgiPlug was added to each well for the final 4 hours of stimulation and cells were analyzed by flow cytometry as described above.

PDTF culture and stimulation

PDTF cultures were performed as described previously[45,46]. Briefly, tumor samples were collected from surgical material of patients with renal cell carcinoma (anti-PD1+anti-CTLA-4 treated n=1 & anti-PD1 treated n=2), ovarian cancer (n=4 & n=1), melanoma (n=7 & n=5), non–small cell lung cancer (n=1 & n=3), and colorectal cancer (n=0 & n=1). Patient characteristics were described previously for samples stimulated with aPD-1 & aCTLA-4 [46] and listed in Supplementary Table 4 for samples stimulated with aPD-1. Definition of responder and non-responder PDTFs were described previously [45,46]. Samples were cut in fragments of 1-2 mm^3 and embedded in an artificial extracellular matrix in a 96-well plate. PDTF cultures were stimulated with medium supplemented with either anti-PD1 alone (nivolumab, Bristol-Myers Squibb) at 10 µg/ml or anti-PD-1 plus anti-CTLA4 (ipilimumab, Bristol-Myers Squibb) at 10 µg/ml where indicated. After 48 hours of culture at 37°C, supernatants were collected and IL-5 levels were measured using the LEGENDplex Human Th Cytokine (BioLegend), according to the manufacturer's protocol.

QUANTIFICATIONS AND STATISTICAL ANALYSIS

Statistical analysis was performed in GraphPad Prism (version 8.4.3) or SPSS Statistics (version 24). All statistical tests were two-sided. All p-values are uncorrected for multiple testing unless stated otherwise. For heatmaps of human flow cytometry data (Figure S1C-F), $\log_2$ transformed cell count/mL or $\log_2$ transformed fold change were depicted, centered around the median for each population (row) separately. Hierarchical clustering was performed on populations and patients based on 1 minus Pearson correlation and Euclidian distance respectively. Complete-linkage was used for both cell populations and patients. To assess dynamics in each cell population analyzed by flow cytometry between baseline and on-nivolumab, the median $\log_2$ fold change from baseline to on-nivolumab ($\log_2$(on-nivolumab) – $\log_2$(pre-nivolumab) was plotted against Benjamini-Hochberg corrected

p-values (Figure 1B). For dynamics in each cell population analyzed by flow cytometry between pre-nivolumab and on-nivolumab, linear modeling was performed (similar to a 2-way ANOVA) to predict $\log_2$ fold changes between pre-nivolumab and on-nivolumab counts / mL based on response and induction treatment: $\log_2$-fold_change ~ response + induction_treatment. This model assumes that the response and induction treatment have an additive and independent effect on log fold changes. For each population responders were contrasted from non-responders. For Figure S2D, the regression coefficients associated with response for each population (x-axis) against the associated (Benjamini-Hochberg corrected) p-values (Wald-test) were plotted. The uncorrected (Wald-test) p-values associated with different induction treatments were estimated. For each population we performed a Shapiro-Wilk normality test on the regression residue to see if the normality assumption was violated.

ADDITIONAL RESOURCES

This paper included flow cytometry and hemocytometer data of blood samples and RNAseq data of tumor biopsies from patients with metastatic TNBC treated in the Netherlands Cancer Institute in the TONIC-trial (NCT02499367). This paper also included hemocytometer data on blood samples generated in the Netherlands Cancer Institute from patients with metastatic NSCLC treated in the PEMBRO-RT trial (NCT02492568), patients with metastatic dMMR tumors treated in the DRUP-trial (NCT02925234), and patients with early-stage colon cancer treated in the NICHE-trial (NCT03026140). Data were kindly provided by the principal investigators of the clinical trials. Further information on the clinical trial procedures and links to clinical publications can be found in the Methods section on clinical trial procedure and Key Resources Table.

KEY RESOURCES TABLE

The Key Resources Table is available in the online version of the paper.

Acknowledgements
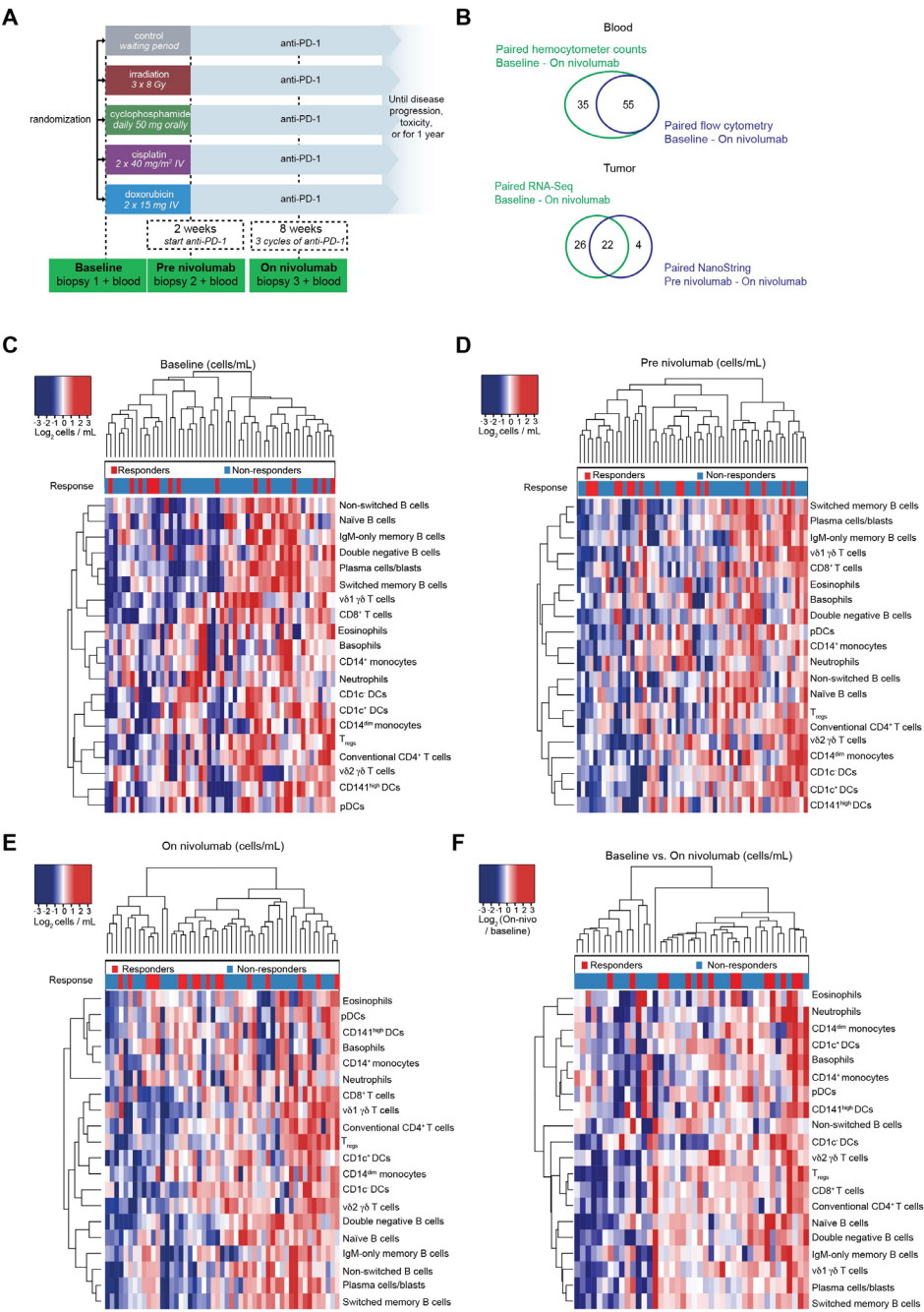
Author Contributions

O.S.B., H.G., L.S., L.V., K.E.d.V and M.K. designed and performed experiments, analyzed and interpreted the data and wrote the manuscript. O.S.B., and L.S. performed the preclinical experiments with contributions from K.Ke., H.G., D.P., C.-S.H., K.V., E.A.M.R., D.K., K.Ko., I.S.A. and R.B., supervised by K.E.d.V.. H.G. performed the blood phenotyping of the TONIC-trial together with N.B., C.K., M.D, M.B., and K.V., supervised by K.E.d.V, and M.K.. L.V. coordinated and analyzed the data of the TONIC-trial of which M.K. is the principal investigator. O.I.I. and E.v.D performed bioinformatic analysis on the RNA-sequencing and blood phenotyping data of the TONIC-trial, respectively. M.C., W.T. and L.H. coordinated trial procedures and collected clinical data of the NICHE-trial, PEMBRO-RT trial and DRUP-trial, respectively. P.B. and E.E.V. are the principal investigators of the PEMBRO-RT and the DRUP-trial, respectively. P.K. & D.S.T. developed and analyzed the data of the PDTF platform. L.F.A.W. supervised bioinformatic and statistical analysis and contributed to interpreting the results. All authors edited and approved the manuscript.

Declaration of interests

O.S.B., H.G., L.S., L.V., O.I.I., E.v.D., N.B., C.K., M.D., K.Ke., M.B., D.P., C.S.H., K.V., E.A.M.R., D.K., L.H., K.Ko., I.S.A., P.K., R.B., and D.S.T. have no competing interests to declare. M.C. reports funding to the institute from BMS and Roche/Genentech and an advisory role for BMS, outside the submitted work. W.T. reports receiving grants from MSD during the conduct of the PEMBRO-RT trial. P.B. reports receiving grants and medication delivery from MSD during the conduct of the PEMBRO-RT trial as well as grants and consultancy fees from BMS outside the submitted work. E.E.V. is legally responsible for all contracts with pharmaceutical companies at the NKI and reports research funding from BMS, outside the submitted work. L.F.A.W. reports funding to the institute from Genmab BV. K.E.d.V. reports research funding from Roche/Genentech and is consultant for Macomics, outside the scope of this work. M.K. reports funding to the institute from BMS, Roche/Genentech, AZ and an advisory role for BMS, Roche, MSD and Daiichi Sankyo, outside the submitted work.

7

Supplemental data

◄◄◄ *Figure S1. Systemic immune cell landscape of patients treated in the TONIC trial at baseline, after induction therapy and on nivolumab, related to Figure 1.* (A) TONIC-trial design (NCT02499367). Patients with metastatic triple-negative breast cancer were randomized to 1 of 4 induction treatment arms (irradiation, cyclophosphamide, cisplatin or doxorubicin) or a two-week waiting period all followed by nivolumab (3mg per kg every 2 weeks) in stage 1 of the trial (19). In stage 2 of the trial, patients were randomized between doxorubicin induction for two weeks followed by nivolumab or immediate start of nivolumab treatment (no induction). 111 patients received at least one cycle of nivolumab (baseline characteristics in Table S1). Blood samples and biopsies were taken at baseline, after 2 weeks of induction treatment and after 3 cycles of nivolumab. Response was determined by iRECIST. (B) Venn diagrams showing the relation in TONIC-trial sample availability between the different analyses. The left panel demonstrates the overlap between availability of paired flow cytometry on fresh blood and paired hemocytometer eosinophil counts from baseline to on-nivo. For 3 patients pre-nivo flow cytometry or hemocytometer data were unavailable due to logistical reasons. The right panel demonstrates overlap between tumor samples available for gene expression analysis by NanoString (pre-nivo – on-nivo) and/or RNA-sequencing (baseline - on-nivo). NanoString analysis was performed on TONIC stage 1 samples, RNA-sequencing on TONIC stage 1 and stage 2. For 4 patients there was only pre-nivo RNA and no baseline RNA available. (C-E) Heatmaps depicting flow cytometry analysis of immune populations at baseline (C), pre-nivo (after induction) (D) and on-nivo (E). Colors in the heatmap correspond to log$_2$ transformed cells/mL and are centered to the median for each population (row) separately. (F) Heatmap representing the log$_2$ fold change of systemic immune cell populations (cells/ml) assessed by flow cytometry from baseline to on-nivo, centered around the median for each immune cell population (row) separately. For (C-F), hierarchical clustering was performed on cell populations and patients based on 1 minus Pearson correlation and Euclidian distance respectively. Complete-linkage was used for both cell populations and patients.

Table S1: Baseline characteristics of all patients receiving at least one dose of nivolumab in the TONIC-trial (stage 1 and 2), related to Figure 1.

	Total population (n = 111)	
Median age, years (range)	52 (29-74)	
WHO performance status, n (%)		
0	70	63%
1	41	37%
gBRCA1/2, n (%)		
Mutation	6	5%
Wildtype	78	70%
Unknown	27	24%
Location of metastasis, n (%)		
Lymph node only	10	9%
Visceral metastasis	79	71%
Other metastasis	22	20%
No. of prior therapies for metastatic disease, n (%)		
0	29	26%
1	56	50%
2-3	26	23%
Previous neoadjuvant or adjuvant therapy, n (%)	96	86%
Previous chemotherapy exposure, n (%)		
Taxane	101	91%
Anthracycline	95	86%
Platinum	60	54%
Capecitabine	60	54%
LDH level, n (%)		
≤ ULN	70	63%
≤ 2x ULN	41	37%

ULN = upper limit of normal (= 250 U/L).

Table S2: Sample availability in the TONIC-trial (stage 1 and 2), related to Figure 1

	# of patients
All included patients	111
Routine eosinophil counts Paired baseline – on-nivo Paired pre-nivo – on-nivo	90 87
Flow cytometry fresh blood Paired baseline – on-nivo Paired pre-nivo – on-nivo	55 52
RNA-sequencing data Paired baseline – on-nivo	48
NanoString gene expression (TONIC stage 1 only) Paired pre-nivo – on-nivo	26

Table S3: List of gene signatures used for human RNA-seq analysis, related to Figure 2.

Gene signature	Genes
Eosinophil gene signature	*SIGLEC8*[87], *RNASE2*[88], *RNASE*[88], *IL5RA*[89], *CCR3*[90]
Expanded T cell signature[32]	CD3D, IDO1, CIITA, CD3E, CCL5, GZMK, CD2, HLA-DRA, CXCL13, IL2RG, NKG7, HLA-E, CXCR6, LAG3, TAGAP, CXCL10, STAT1, GZMB
Structural CD8+ T cell signature	*CD3D*[91], *CD3E*[91], *CD3G*[91], *CD8A*[92], *CD8B*[92], *TRA*[91], *TRBC1*[91], *TRBC2*[91], *CD247*[91]
IFNγ gene signature[33]	IDO1, CXCL9, CXCL10, HLA-DRA, STAT1, IFNG

Table S4. Patient characteristics of tumors included in PDTF analysis treated with aPD-1 alone. Related to Figure 5.

Patient ID	Tumor type	Tumor site	Ex vivo response to aPD-1
CRC003	Colorectal cancer	Primary	Yes
OV013-3	Ovarian cancer	Peritoneal metastasis	Yes
LU019	Non-small cell lung cancer	Primary	Yes
AKB803	Melanoma	Lymph node metastasis	Yes
MEL021	Melanoma	Lung metastasis	Yes
MEL025-1	Melanoma	Lymph node metastasis	No
LU027-2	Non-small cell lung cancer	Primary	No
MEL032	Melanoma	Metastasis muscle	No
RE015	Renal cell carcinoma	Primary	No
RE028	Renal cell carcinoma	Primary	No
MEL072	Melanoma	Lymph node metastasis	No
LU032	Non-small cell lung cancer	Primary	No
MEL077	Melanoma	Abdominal metastasis	No
LU028	Non-small cell lung cancer	Primary	No

7

regression coefficient on the effect of response by changes in immune populations analyzed by flow cytometry (pre-nivo to on-nivo; x-axis) and Benjamini-Hochberg corrected p-values (y-axis), while respecting additive influence of induction treatment (linear modeling). The regression coefficients associated with response for each population (x-axis) against the associated (Benjamini-Hochberg corrected) p-values (Wald-test) were plotted. (E) Induction treatment effect on eosinophil dynamics as determined by flow cytometry shown as median count and interquartile range, statistical analysis was performed using Wilcoxon Signed-Rank test comparing baseline to on-nivo in responders and non-responders. (F) Paired flow cytometry analysis of eosinophils (log2 transformed cells/ml) comparing pre-nivo to on-nivo in responders and non-responders, treated in the TONIC-trial. Paired data was available for 52 patients. Statistics by Wilcoxon Signed-Rank. (G) Fold change in systemic eosinophils assessed by hemocytometer from baseline to on-nivo in responders and non-responders. Paired data is available for 90 patients. Statistics by Mann-Whitney, median with interquartile range (IQR). (H) Paired hemocytometer analysis of systemic eosinophils comparing pre-nivo to on-nivo in responders and non-responders. Paired data is available for 87 patients. Statistics by Wilcoxon Signed-Rank. (I-J) Kaplan-Meier curve of progression-free survival (I) or overall survival (J) of patients divided between a fold change in eosinophils (pre-nivo to on nivo) lower than 2 or equal to/higher than 2. Statistics with log-rank and univariate hazard ratios by Cox regression (fold change lower than 2 as reference category). Data was cut-off at 1 March 2021.
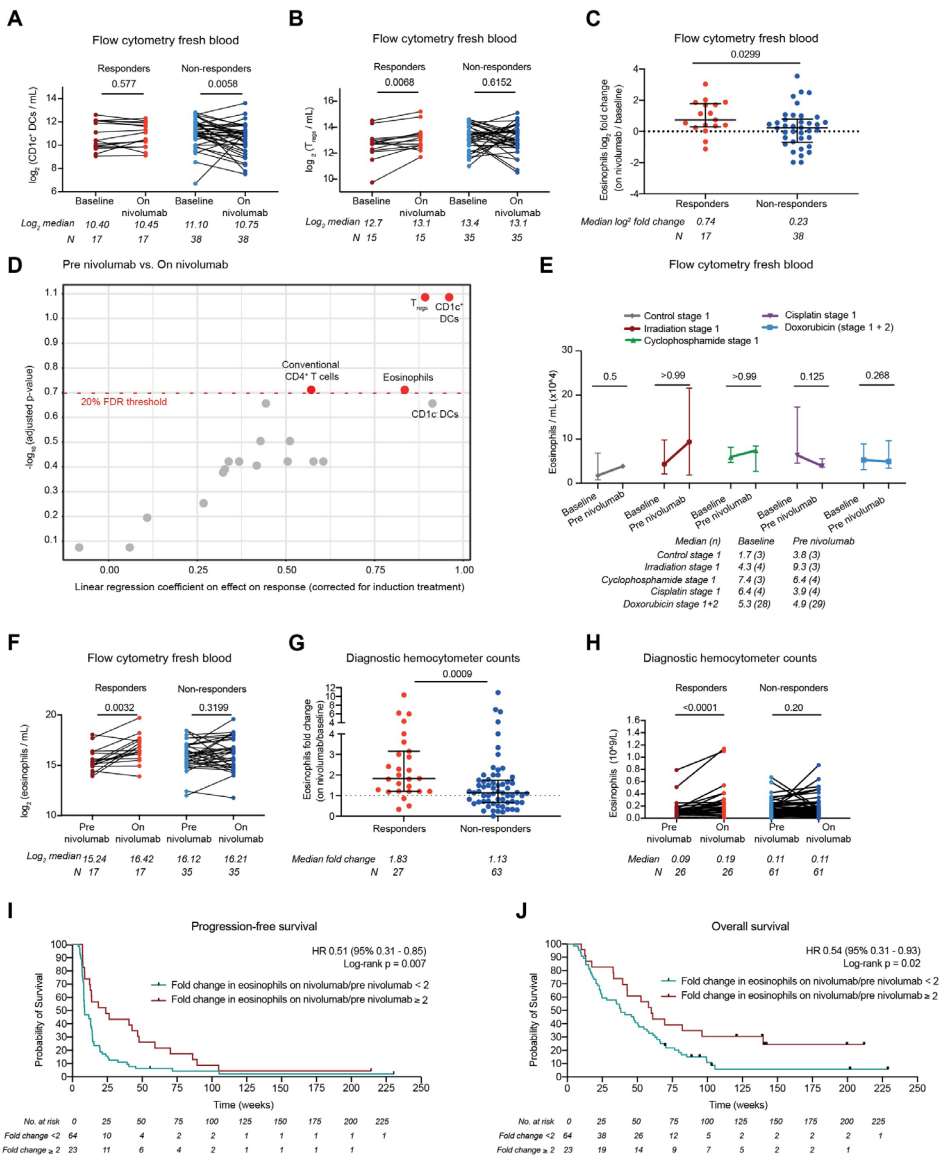
Figure S2. Systemic reduction of CD1c⁺ dendritic cells and expansion of T_{regs} and eosinophils during immune checkpoint blockade response is independent of induction treatment in TONIC trial, related to Figure 1. (A-B) Paired flow cytometry analysis of systemic CD1c⁺ DCs (log2 transformed cells/ml) (A) and T_{regs} (log2 transformed cells/ml) (B) comparing baseline to on-nivo in responders and non-responders, treated in the TONIC-trial. Paired data are available for 55 patients (A) and (B). Statistics by Wilcoxon Signed-Rank. (C) Fold change in systemic eosinophils (log2 transformed cells/ml by flow cytometry) from baseline to on-nivo in responders and non-responders, treated in the TONIC-trial. Paired data is available for 55 patients. Statistics by Mann-Whitney, median with interquartile range (IQR). (D) Volcano plot depicting the linear

proficient (pMMR) (D) and mismatch repair deficient (dMMR) (E) early-stage colon cancer, treated with two cycles of neo-adjuvant nivolumab and ipilimumab in the NICHE-trial. (F) Fold change of eosinophil counts after two or three cycles of nivolumab treatment in patients with metastatic dMMR tumors, treated with nivolumab (240 mg, q2w) in the dMMR cohort of the Drug Rediscovery Protocol (NCT02925234)[31]. 7 patients with colorectal cancer (6 patients with paired data), 1 patient with urothelial cell cancer (no paired data), 1 patient with cervical cancer, 1 patient with breast cancer and 1 patient with endometrial cancer were included in this cohort. (G) Paired analysis of absolute eosinophil counts between baseline and two or three cycles of nivolumab in responding and non-responding patients with metastatic dMMR tumors, treated with nivolumab in the dMMR cohort of the Drug Rediscovery Protocol. Response was defined as complete response (CR), partial response (PR) or stable disease (SD) for 24 weeks or longer according to RECIST1.1 for (A-B and F-G). For (A,C,F), median and interquartile ranges are displayed; statistics by Mann-Whitney. For (B-E & G), statistics by Wilcoxon-signed-rank. Dashed lines indicate the threshold (0.1 x10^9 cells/L) of the hemocytometer counts reported in the patient records, counts below this threshold were replaced with a value of 0.09 x10^9 cells/L.
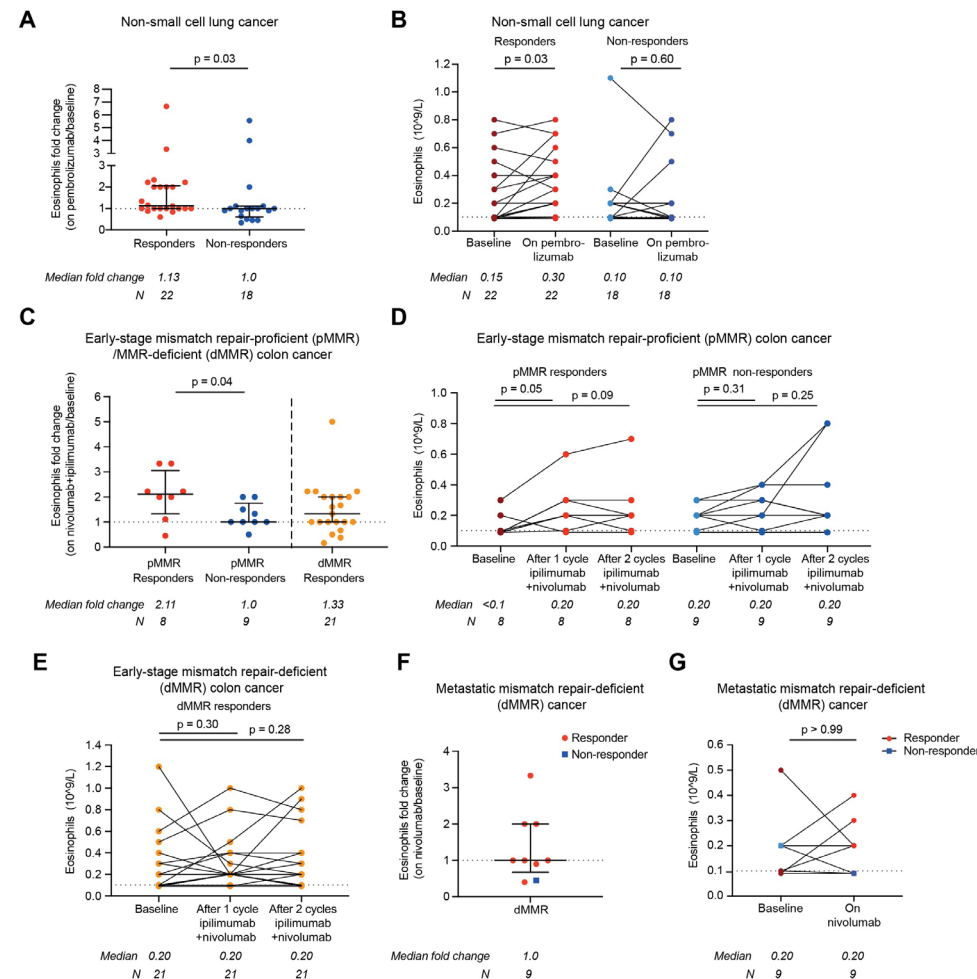
Figure S3. Systemic eosinophil accumulation after ICB and association with therapy response in different cancer types, related to Figure 1. (A) Fold change of eosinophil counts after two cycles of pembrolizumab in patients with metastatic non-small lung cancer (NSCLC) treated with pembrolizumab (200 mg, q3w) with or without upfront radiation (NCT02492568)[29]. Paired data was available for 40 patients. (B) Paired analysis of absolute eosinophil counts in blood between baseline and two cycles of pembrolizumab in responding and non-responding patients with metastatic NSCLC. (C) Fold change of eosinophil counts after one cycle of ipilimumab/ nivolumab treatment and baseline in patients with early-stage colon cancer, either mismatch repair-proficient (pMMR) or mismatch repair deficient (dMMR), treated with neo-adjuvant nivolumab (day 1 and day 15, 3 mg/kg) and ipilimumab (day 1, 1 mg/kg) in the NICHE-trial (NCT03026140)[30]. Response was defined as a pathological response (<90% tumor rest). Eosinophils were measured after 1 cycle of ipilimumab/nivolumab and after 1 additional cycle of nivo. All patients with early-stage dMMR colon cancer had a pathological response. Paired data was available for 21 patients. (D-E) Paired analysis of absolute eosinophil counts in blood between baseline and on treatment in responding and non-responding patients with mismatch repair-

transformed data are presented. Mean ±S.E.M., 1-way ANOVA followed by Dunnett's multiple comparisons test. (E) Frequency of effector CD8+ (left), effector CD4+ CD25- (middle) T cells and IFNg+ and TNFa+ double positive CD8+ T cells (right) in blood of KEP mice at tumor-related endpoint (n=4-5), determined by flow cytometry. Mean ±S.E.M., 1-way ANOVA followed by Dunnett's multiple comparisons test. (F) Frequency of eosinophils (defined as: CD11b+ Ly6G^{low} F4/80^{int} SiglecF+) in the TDLN (left) and spleen (right) of KEP mice at tumor-related endpoint as determined by flow cytometry (n=4-6). Mean ±S.E.M., 1-way ANOVA followed by Dunnett's multiple comparisons test. (G) Representative image and quantification of immunohistochemical staining for major basic protein (MBP) of KEP tumors at tumor-related endpoint demonstrating eosinophil distribution in intratumoral, periphery and border regions. Intratumoral areas were defined as more than 700μm distant from the border of the tumor tissue; tumor periphery was defined as areas between 200μm and 700μm from the border of tumor tissue; border areas were defined as areas spanning from 200μm inside the tumor tissue to 300μm into the surrounding non-tumoral tissue. Scale bar represents 100μm. Each dot represents the average of 4-5 different tumor areas of 0.5mm² per mouse. Mean ±S.E.M., Kruskal-Wallis test. (H) Volcano plot demonstrating differentially expressed genes between eosinophils sorted from the blood of mice treated with Ctrl Ab or CIS + ICB in responsive phase of therapy. Genes contributing to the "Hallmark_Interferon_gamma_ response" and "Hallmark_oxidative_phosphorylation" gene-sets are highlighted. (I) Gene sets derived from the Molecular Signatures Database Hallmark Gene Set Collection enriched in mice treated with CIS + ICB (blue) or Ctrl Ab (orange) (FDR q < 0,25). The Normalized Enrichment Scores (NES) of the top 10 enriched gene sets are shown, ordered based on ascending q-value. (J) Enrichment plot for the gene-set "Hallmark_Interferon_gamma_response" upregulated in eosinophils treated with CIS + ICB. (K) Enrichment plot for the gene-set "Hallmark_oxidative_ phosphorylation" upregulated in eosinophils treated with Ctrl Ab. ns, not significant *p<0.05, **p<0.01, ***p<0.001, ****p<0.0001.
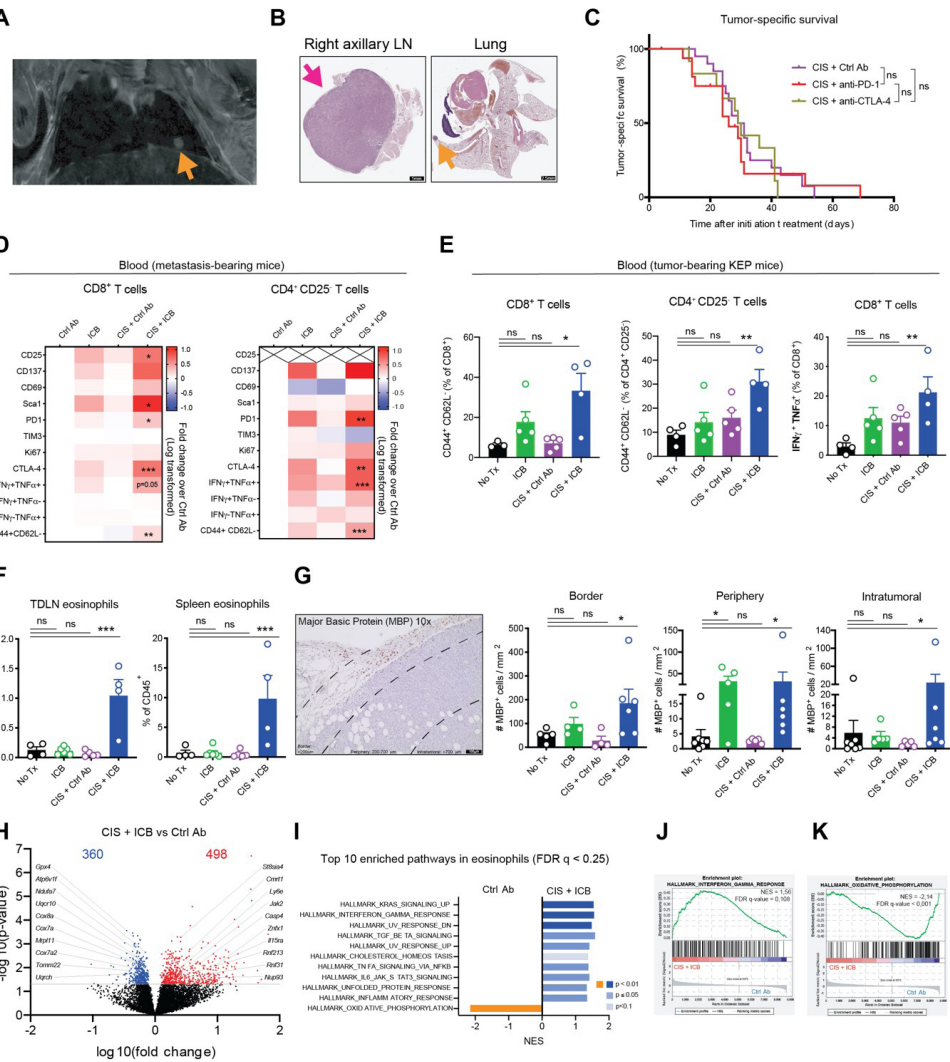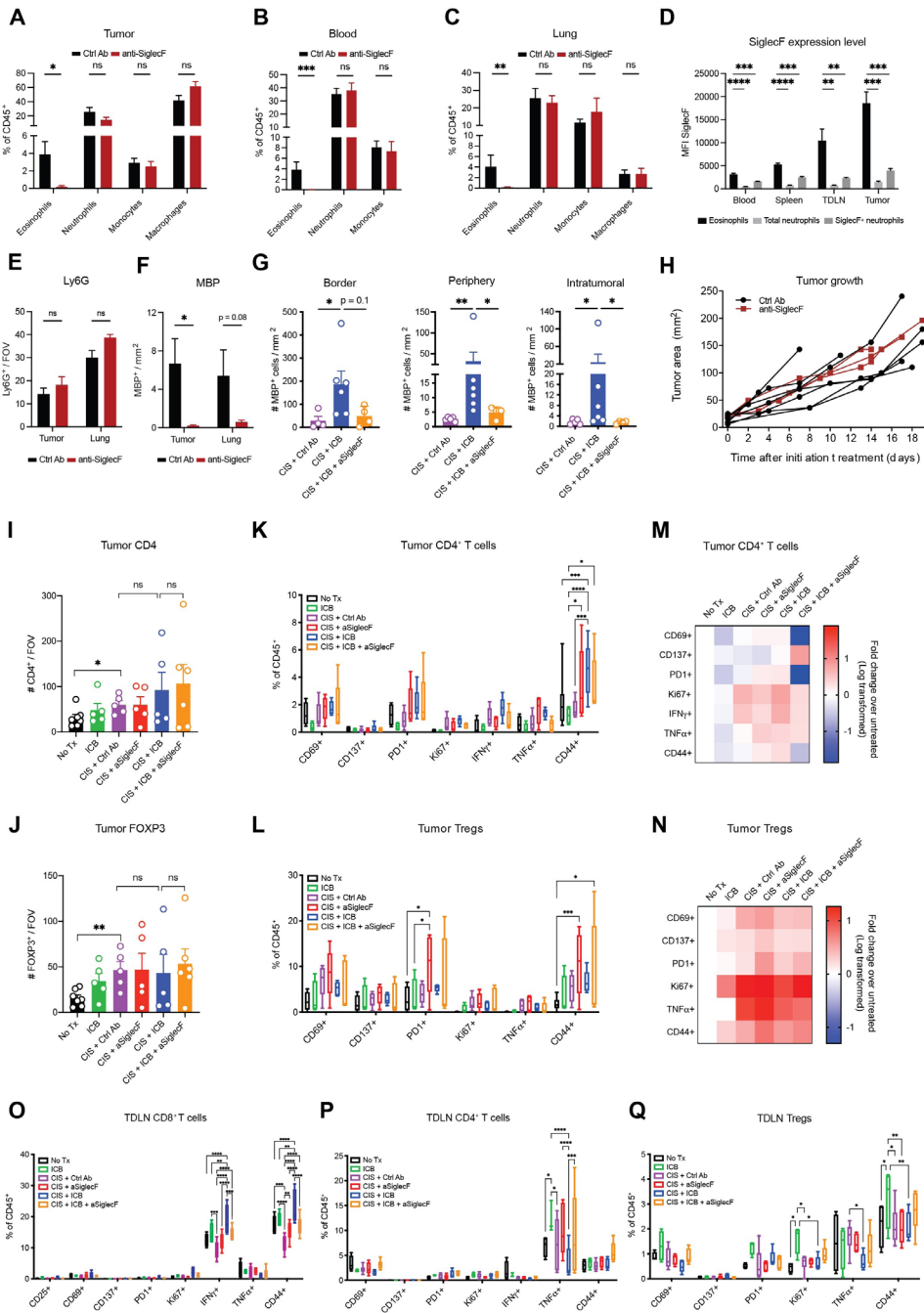
Figure S4. ICB and cisplatin induces systemic T-cell activation and eosinophil expansion in pre-clinical models of mammary tumorigenesis and advanced metastatic breast cancer, related to Figure 3. (A-B) MRI images displaying the lung and axillary lymph nodes (A) and H&E staining of right axillary lymph node (= primary tumor draining lymph node) and lungs (B) of mice bearing KEP-derived metastases 15 days after mastectomy. Scale bars represent 1mm (left) and 2.5mm (right). Orange arrows indicate lung metastatic nodules and pink arrows indicate a lymph node affected by metastatic disease. (C) Kaplan-Meier survival curves of KEP mice treated as indicated (CIS + Ctrl Ab, n=22, 3 censored, CIS + anti-CTLA-4, n=12, 1 censored, or CIS + anti-PD-1, n=17, 3 censored). Log-rank (Mantel-Cox) test. (D) Fold change compared to Ctrl Ab-treated mice of CD8+ (left) and CD4+ CD25- (right) T cells expressing the indicated activation markers expressed in blood at metastasis-related endpoint (n=4-7), determined by flow cytometry. Log

◄◄◄ *Figure S5. Depletion of eosinophils using anti-SiglecF antibody does not promote CD4+ T cell or T$_{reg}$ activation in the tumor and tumor-draining lymph node during combined ICB and cisplatin treatment, related to Figure 4. (A-C) Frequency of indicated immune cells in the tumor (A), blood (B), and lungs (C) of treated KEP mice at tumor-related endpoint as determined by flow cytometry (n=4-10). Mean ±S.E.M., Mann-Whitney. (D) Mean Fluorescence Intensity (MFI) of SiglecF expression on eosinophils, total neutrophils or SiglecF+ neutrophils of KEP mice at tumor-related endpoint (n=4), measured by flow cytometry in indicated tissues. Mean ±S.E.M., Multiple unpaired t-tests followed by Holm-Sidak for multiple comparison. (E) Quantification of IHC staining for Ly6G+ cells per FOV in the tumor and lung of treated KEP mice at tumor-related endpoint (n=6-10 mice, the average of 5 FOVs per mouse). (F) Quantification of IHC staining for MBP+ cells per mm² in the tumor and lung of treated KEP mice at tumor-related endpoint (n=4-5 mice). (G) Quantification of IHC staining for MBP of KEP tumors at tumor-related endpoint demonstrating eosinophil distribution in intratumoral (left), periphery (middle) and border regions (right), defined and analyzed as described in Figure S4G. Data of CIS + Ctrl Ab and CIS + ICB groups are the same as displayed in Figure S4G. Mean ±S.E.M., Mann-Whitney. (H) Growth curve of mammary tumors in KEP mice treated with control antibody (n=7) or anti-SiglecF (n=3). (I-Q) KEP mice were sacrificed 21 days after start of treatment (responsive phase). Untreated KEP mice were analyzed 21 days after they reached a tumor area of 50 mm², or when the tumors reached an area of 225 mm². (I-J) Number of tumor-infiltrating CD4+ (I) and FOXP3+ (J) cells in 'responsive phase' of treatment, quantified by IHC (n=5-7 mice per group. For each mouse, the average of 5-9 FOVs ±S.E.M is displayed). Student's t-test. (K-L) Frequency of tumor-infiltrating CD4+CD25- T cells (K) and regulatory T cells (L) expressing the indicated activation markers as determined by flow cytometry, measured 21 days after initiation of indicated treatments (n=5). (M-N) Data of (K-L) was normalized to the frequency observed in control mice. Log transformed data is presented. (O-Q) Frequency of CD8+ T cells (O), CD4+CD25- T cells (P) and regulatory T cells (Q) expressing the indicated activation markers as determined by flow cytometry in the TDLN, measured 21 days after initiation of indicated treatments (n=5). Boxes represent median and interquartile range; whiskers represent full range. 2-way ANOVA followed by Tukey's multiple comparison test. *p<0.05, **p<0.01, ***p<0.001, ****p<0.0001.*
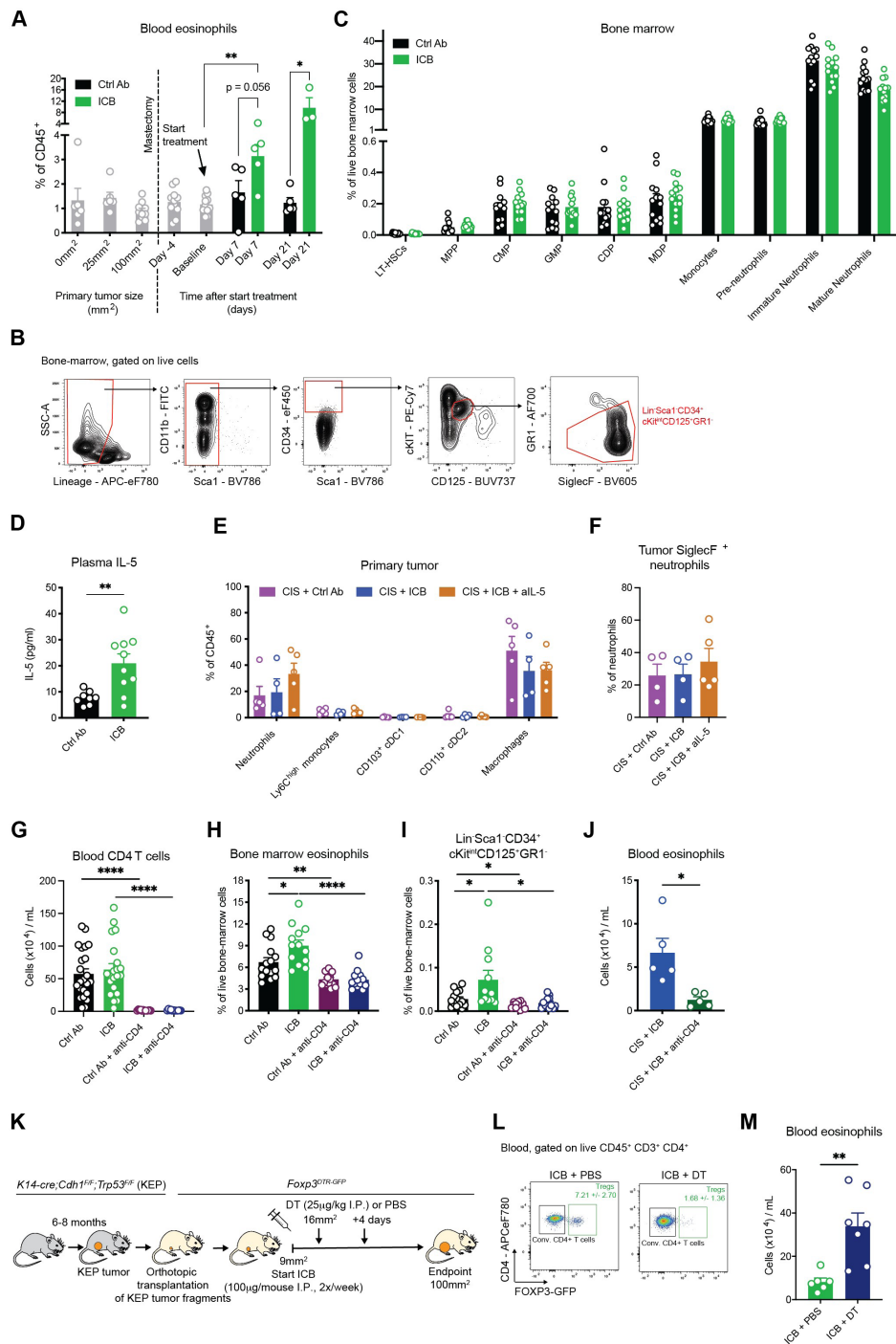
◀◀◀ **Figure S6. Dynamics and properties of ICB-induced eosinophils in mice with KEP-derived metastatic disease or mammary tumors, related to Figure 5.** (A) Frequency of eosinophils in blood of mice with KEP-derived metastatic disease treated as described in Figure 3E, as determined by flow cytometry at the indicated time-points (Ctrl Ab n=3-11, ICB n=3-11). (B) Gating strategy for the identification of Lin⁻Sca1⁻CD34⁺cKitInt CD125⁺Gr1⁻ eosinophil progenitors in the bone marrow. (C) Frequency of indicated cell types in the bone marrow of mice with KEP-derived metastatic disease treated as indicated, as determined by flow cytometry (Ctrl Ab n=13, ICB n=13). LT-HSC, long-term hematopoietic stem cell; MPP, multipotent progenitor; CMP, common myeloid progenitor; GMP, granulocyte-monocyte progenitor; CDP, common dendritic cell progenitor; MDP, macrophage-dendritic cell progenitors. Multiple unpaired t-tests followed by Holm-Sidak for multiple comparison. (D) Absolute quantification of IL-5 levels in plasma of mice with KEP-derived metastatic disease treated as indicated (Ctrl Ab n=9, ICB n=10) as measured by Legend Plex. The mice shown here are the same used for the analysis of Figure 5F. (E) Frequency of indicated immune cell populations in tumors of treated KEP mice at tumor-related endpoint, as determined by flow cytometry (n=4-5). The mice shown here are the same used for the analysis of Figure 5K-N. 1-way ANOVA. (F) Frequency of SiglecF+ neutrophils in primary tumor of treated KEP mice at tumor-related endpoint, as determined by flow cytometry (n=4-5). (G) Number of CD4 T cells (gated as: CD3⁺CD8⁻CD25⁻ cells) in the blood of mice with KEP-derived metastatic disease treated as described in Figure 5R, as determined by flow cytometry. Pooled data of two independent experiments. (H-I) Frequency of total eosinophils (H) and Lin⁻Sca1⁻CD34⁺cKitInt CD125⁺Gr1⁻ eosinophil progenitors (I) in the bone marrow of mice with KEP-derived metastatic disease treated as described in Figure 5R, as determined by flow cytometry (n=13-14). (J) Number of eosinophils in the blood of KEP-metastasis-bearing mice treated with CIS+ICB (n=5) or CIS+ICB+anti-CD4 (n=5) and analyzed on day 10 after start of treatment. (K) Experimental set-up and treatment scheme for the depletion of T_{regs} in mice with KEP-derived orthotopic mammary tumors. (L) Representative dot plots showing T_{reg} levels in the blood of mice at the experimental endpoint. Average frequency of T_{regs} as percentage of CD4⁺ cells ±S.E.M. are displayed. DT, diphtheria toxin. (M) Number of eosinophils in blood of mice treated as described in (H) (ICB + PBS, n=6, ICB + DT n=7), as determined by flow cytometry. All data are mean ±S.E.M, unpaired t-test, unless indicated otherwise. ns, not significant, *p<0.05, **p<0.01, ****p<000.1.
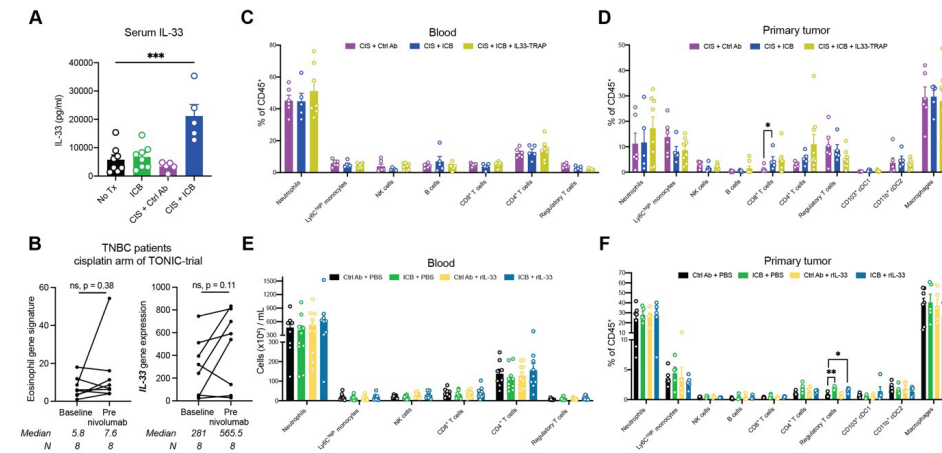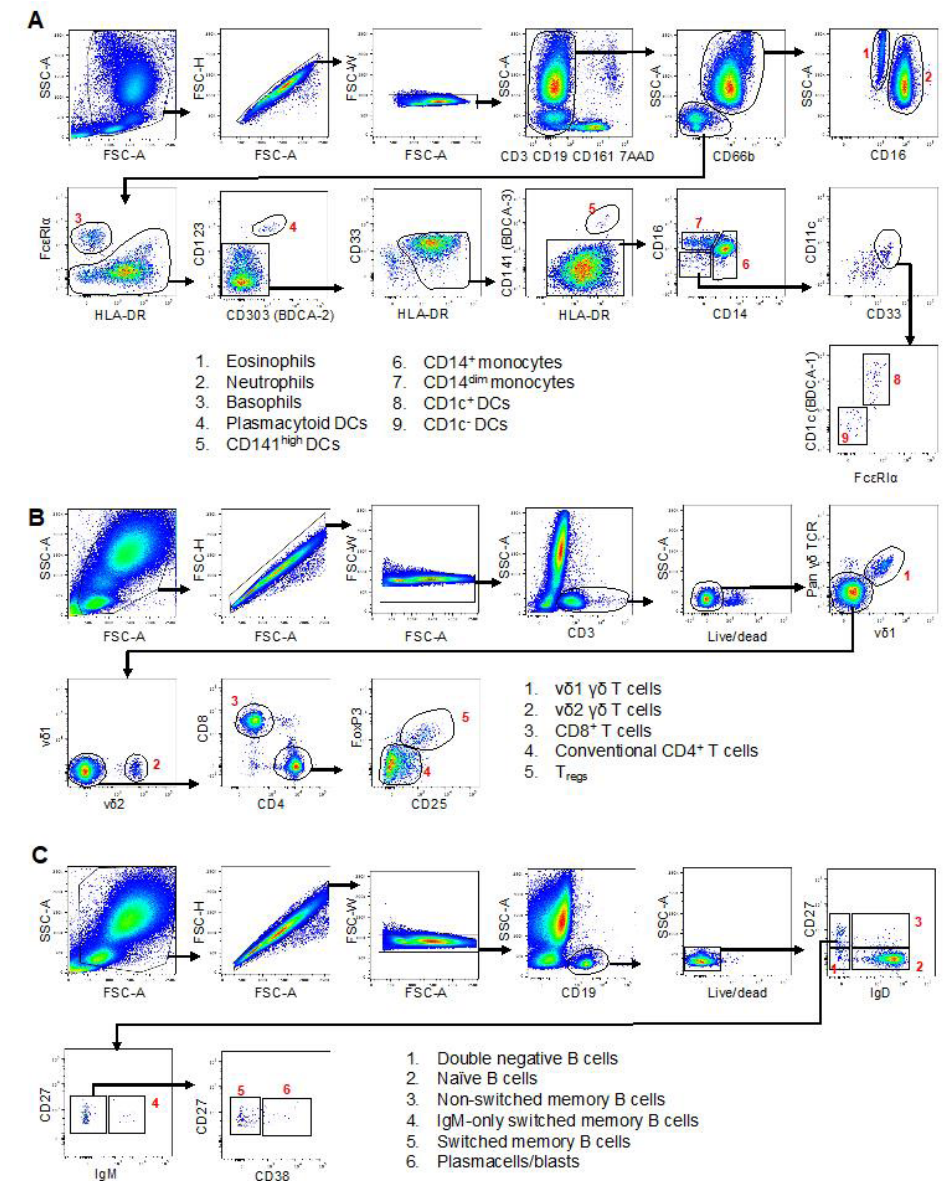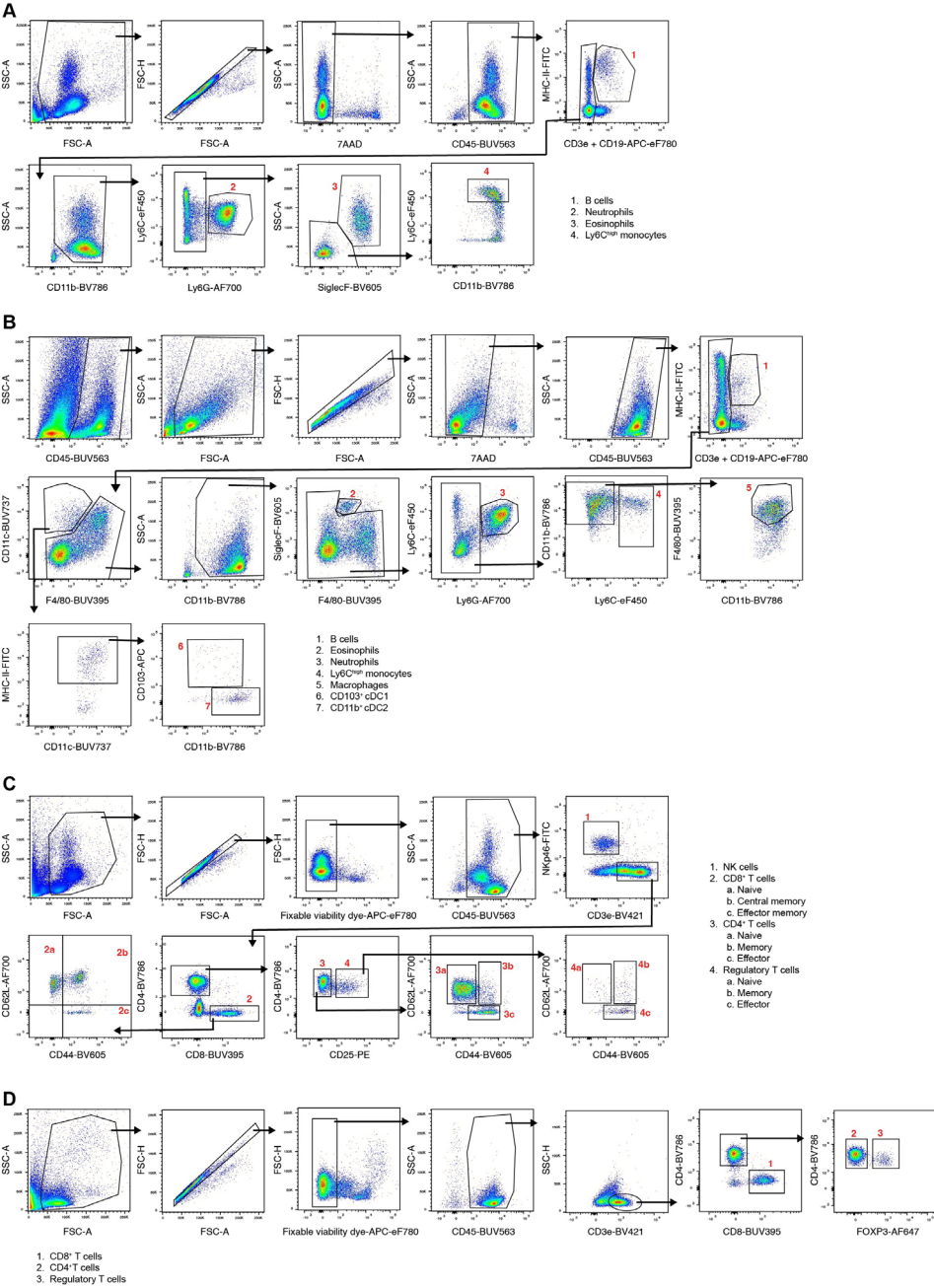
Figure S7. ICB and rIL-33 specifically promote the expansion and activation of eosinophils in mice with mammary tumors, related to Figure 6 and 7. (A) IL-33 levels in serum determined by Legend Plex of KEP mice at tumor-related endpoint treated as indicated (n=5-8). **(B)** Eosinophil gene signature (left) and IL33 gene expression (right) from RNA-seq analysis of metastatic lesions of TNBC patients treated in the cisplatin arm of the TONIC trial. **(C-D)** Frequency of indicated immune cell populations in the blood **(C)** and primary tumor **(D)** as determined by flow cytometry of KEP mice treated as described in Figure 6D-F (n=5-8). **(E-F)** Frequency of indicated immune cell populations in the blood (n=8-10) **(E)** and primary tumor (n=5-7) **(F)** determined by flow cytometry of mice bearing orthotopically transplanted KEP tumors in responsive phase of therapy (i.e. tumor area of 150mm^2) and treated as described in Figure 7. Statistical analysis performed by 1-way ANOVA or Kruskal-Wallis followed by Dunnett's or Dunn's multiple comparisons test, comparing each group against control mice, for each immune population. All data are mean ±S.E.M., *p<0.05, **p<0.01, ***p<0.001.

Figure S8. Gating strategy for flow cytometry analysis of human peripheral blood immune populations, related to STAR Methods. (A) Myeloid panel gating strategy identifying eosinophils (lineage-, high side scatter, CD66b+, CD16-), neutrophils (lineage-, high side scatter, CD66b+, CD16+), basophils (lineage-, low side scatter, CD66b-, HLA-DR-, FceRIa+), plasmacytoid DCs (lineage-, low side scatter, CD66b-, HLA-DR+, CD303+, CD123+), CD141high DCs (lineage-, low side scatter, CD66b-, HLA-DR+, CD33+, CD141+), CD14+ monocytes (lineage-, CD66b-, HLA-DR+, CD33+, CD14+), CD14dim monocytes (lineage-, CD66b-, HLA-DR+, CD33+, CD14dim, CD16+), CD1c+ DCs (lineage-, CD66b-, HLA-DR+, CD33+, CD14- , CD16-, CD1c+, FceRIa+) and CD1c- DCs (lineage-, CD66b-, HLA-DR+, CD33+, CD14- , CD16-, CD1c-, FceRIa-). **(B)** T cell panel gating strategy to identify vd1 gd T cells (CD3+, vd1+, pan gd TCR+), vd2 gd T cells (CD3+, vd2+), CD8 T cells (CD3+, vd1-, pan gd TCR-, vd2-, CD8+, CD4-), conventional CD4 T cells (CD3+, vd1-, pan gd TCR-, vd2-, CD8-, CD4+, FoxP3-) and Tregs (CD3+, vd1-, pan gd TCR-, vd2-, CD8-, CD4+, FoxP3+, CD25high). **(C)** Gating strategy to identify B cell subsets identifying double negative B cells (CD19+, CD27-, IgD-), naïve B cells (CD19+, CD27-, IgD+), non-switched memory B cells (CD19+, CD27+, IgD+), IgM-only memory B cells (CD19+, CD27+, IgD-, IgM+), switched memory B cells (CD19+, CD27+, IgD-, IgM-, CD38-/+), and plasmacells/blasts (CD19+, CD27+, IgD-, IgM-, CD38high). ▶▶▶

◀◀◀ *Figure S9. Gating strategy for flow cytometry to identify immune cell populations in mouse blood and tumor, related to STAR Methods.* (A-B) Myeloid panel gating strategy for blood (A) and tumor (B) samples identifying B cells (CD45+, CD19+, MHC-II+), neutrophils (CD45+, CD3-, CD19-, CD11b+, Ly6g+), eosinophils (in blood: CD45+, CD3-, CD19-, Ly6g-, CD11b+, SSC-Ahigh, SiglecF+; in tumor: CD45+, CD3-, CD19-, CD11b+, SiglecF+, F4/80int), Ly6chigh monocytes (CD45+, CD3-, CD19-, Ly6g-, SiglecF-, CD11b+, Ly6chigh), macrophages (in tumor:, CD45+, CD3-, CD19-, SiglecF-, Ly6g-, Ly6c-, CD11b+, F4/80high), CD103+ cDC1 (in tumor: CD45+, CD3-, CD19-, F4/80-, CD11c+, MHC-II+ CD11blow, CD103+) and CD11b+ cDC2 (in tumor: CD45+, CD3-, CD19-, F4/80-, CD11c+, MHC-II+, CD103-, CD11b+).

(C-D) Lymphoid panel gating strategy in blood analyzed unfixed (C) and fixed (D) identifying NK cells (unfixed: CD45+, CD3-, NKp46+), naïve CD8+ T cells (unfixed: CD45+, NKp46-, CD4-, CD3+, CD8+; CD44-, CD62L+), central memory CD8+ T cells (unfixed: CD45+, NKp46-, CD4-, CD3+, CD8+, CD44+, CD62L+), effector memory CD8+ T cells (unfixed: CD45+, NKp46-, CD4-, CD3+, CD8+, CD44+, CD62L-), total CD8+ T cells (fixed: CD45+, CD4-, CD3+, CD8+), naïve CD4+ T cells (unfixed: CD45+, NKp46-, CD8-, CD25-, CD3 +, CD4+, CD44-, CD62L+), memory CD4+ T cells (unfixed: CD45+, NKp46-, CD8-, CD25-, CD3+, CD4+, CD44+, CD62L+), effector CD4+ T cells (unfixed: CD45+, NKp46-, CD8-, CD25-, CD3+, CD4+, CD44+, CD62L-), total CD4+ T cells (fixed: CD45+, CD8-, FOXP3-, CD3+, CD4+), naïve Tregs (unfixed: CD45+, NKp46-, CD8-, CD25+, CD3+, CD4+, CD44-, CD62L+), memory Tregs (unfixed: CD45+, NKp46-, CD8-, CD25+, CD3+, CD4+, CD44+, CD62L+), effector Tregs (unfixed: CD45+, NKp46-, CD8-, CD25+, CD3+, CD4+, CD44+, CD62L-) and total Tregs (fixed: CD45+, CD8-, FOXP3+, CD3+, CD4+).

References

1.   Adams, S., Schmid, P., Rugo, H.S., Winer, E.P., Loirat, D., Awada, A., Cescon, D.W., Iwata, H., Campone, M., Nanda, R., et al. (2019). Pembrolizumab monotherapy for previously treated metastatic triple-negative breast cancer: cohort A of the phase II KEYNOTE-086 study. Annals of Oncology 30, 397-404. 10.1093/annonc/mdy517.

2.   Winer, E.P., Lipatov, O., Im, S.A., Goncalves, A., Muñoz-Couselo, E., Lee, K.S., Schmid, P., Tamura, K., Testa, L., Witzel, I., et al. (2021). Pembrolizumab versus investigator-choice chemotherapy for metastatic triple-negative breast cancer (KEYNOTE-119): a randomised, open-label, phase 3 trial. Lancet Oncol 22, 499-511. 10.1016/s1470-2045(20)30754-3.

3.   Schmid, P., Rugo, H.S., Adams, S., Schneeweiss, A., Barrios, C.H., Iwata, H., Diéras, V., Henschel, V., Molinero, L., Chui, S.Y., et al. (2020). Atezolizumab plus nab-paclitaxel as first-line treatment for unresectable, locally advanced or metastatic triple-negative breast cancer (IMpassion130): updated efficacy results from a randomised, double-blind, placebo-controlled, phase 3 trial. The Lancet. Oncology 21, 44-59. 10.1016/S1470-2045(19)30689-8.

4.   Cortes, J., Cescon, D.W., Rugo, H.S., Nowecki, Z., Im, S.A., Yusof, M.M., Gallardo, C., Lipatov, O., Barrios, C.H., Holgado, E., et al. (2020). Pembrolizumab plus chemotherapy versus placebo plus chemotherapy for previously untreated locally recurrent inoperable or metastatic triple-negative breast cancer (KEYNOTE-355): a randomised, placebo-controlled, double-blind, phase 3 clinical trial. Lancet 396, 1817-1828. 10.1016/s0140-6736(20)32531-9.

5.   Demaria, O., Cornen, S., Daëron, M., Morel, Y., Medzhitov, R., and Vivier, E. (2019). Harnessing innate immunity in cancer therapy. Nature 574, 45-56. 10.1038/s41586-019-1593-5.

6.   Grisaru-Tal, S., Itan, M., Klion, A.D., and Munitz, A. (2020). A new dawn for eosinophils in the tumour microenvironment. Nat Rev Cancer 20, 594-607. 10.1038/s41568-020-0283-9.

7.   Grisaru-Tal, S., Rothenberg, M.E., and Munitz, A. (2022). Eosinophil-lymphocyte interactions in the tumor microenvironment and cancer immunotherapy. Nat Immunol 23, 1309-1316. 10.1038/s41590-022-01291-2.

8.   Rosenberg, H.F., Dyer, K.D., and Foster, P.S. (2013). Eosinophils: changing perspectives in health and disease. Nat Rev Immunol 13, 9-22. 10.1038/nri3341.

9.   Kratochvill, F., Neale, G., Haverkamp, J.M., Van de Velde, L.A., Smith, A.M., Kawauchi, D., McEvoy, J., Roussel, M.F., Dyer, M.A., Qualls, J.E., and Murray, P.J. (2015). TNF Counterbalances the Emergence of M2 Tumor Macrophages. Cell Rep 12, 1902-1914. 10.1016/j.celrep.2015.08.033.

10.   Zaynagetdinov, R., Sherrill, T.P., Gleaves, L.A., McLoed, A.G., Saxon, J.A., Habermann, A.C., Connelly, L., Dulek, D., Peebles, R.S., Jr., Fingleton, B., et al. (2015). Interleukin-5 facilitates lung metastasis by modulating the immune microenvironment. Cancer Res 75, 1624-1634. 10.1158/0008-5472.can-14-2379.

11.   Carretero, R., Sektioglu, I.M., Garbi, N., Salgado, O.C., Beckhove, P., and Hammerling, G.J. (2015). Eosinophils orchestrate cancer rejection by normalizing tumor vessels and enhancing infiltration of CD8(+) T cells. Nature immunology 16, 609-617. 10.1038/ni.3159.

12.   Jia, S., Li, W., Liu, P., and Xu, L.X. (2019). A role of eosinophils in mediating the anti-tumour effect of cryo-thermal treatment. Sci Rep 9, 13214. 10.1038/s41598-019-49734-5.

13.   Arnold, I.C., Artola-Boran, M., Gurtner, A., Bertram, K., Bauer, M., Frangez, Z., Becher, B., Kopf, M., Yousefi, S., Simon, H.U., et al. (2020). The GM-CSF-IRF5 signaling axis in eosinophils promotes antitumor immunity through activation of type 1 T cell responses. J Exp Med 217, e20190706. 10.1084/jem.20190706.

14.   Hollande, C., Boussier, J., Ziai, J., Nozawa, T., Bondet, V., Phung, W., Lu, B., Duffy, D., Paradis, V., Mallet, V., et al. (2019). Inhibition of the dipeptidyl peptidase DPP4 (CD26) reveals IL-33-dependent eosinophil-mediated control of tumor growth. Nature immunology 20, 257-264. 10.1038/s41590-019-0321-5.

15.   Reichman, H., Itan, M., Rozenberg, P., Yarmolovski, T., Brazowski, E., Varol, C., Gluck, N., Shapira, S., Arber, N., Qimron, U., et al. (2019). Activated Eosinophils Exert Antitumorigenic Activities in Colorectal Cancer. Cancer Immunol Res 7, 388-400. 10.1158/2326-6066.CIR-18-0494.

16.   Andreone, S., Spadaro, F., Buccione, C., Mancini, J., Tinari, A., Sestili, P., Gambardella, A.R., Lucarini, V., Ziccheddu, G., Parolini, I., et al. (2019). IL-33 Promotes CD11b/CD18-Mediated Adhesion of Eosinophils to Cancer Cells and Synapse-Polarized Degranulation Leading to Tumor Cell Killing. Cancers (Basel) 11, 1664. 10.3390/cancers11111664.

17.   Varricchi, G., Galdiero, M.R., Loffredo, S., Lucarini, V., Marone, G., Mattei, F., and Schiavoni, G. (2018). Eosinophils: The unsung heroes in cancer? Oncoimmunology 7, e1393134. 10.1080/2162402x.2017.1393134.

18.   Grisaru-Tal, S., Dulberg, S., Beck, L., Zhang, C., Itan, M., Hediyeh-Zadeh, S., Caldwell, J., Rozenberg, P., Dolitzky, A., Avlas, S., et al. (2021). Metastasis-Entrained Eosinophils Enhance Lymphocyte-Mediated Antitumor Immunity. Cancer Res 81, 5555-5571. 10.1158/0008-5472.can-21-0839.

19.   Simon, S.C.S., Hu, X., Panten, J., Grees, M., Renders, S., Thomas, D., Weber, R., Schulze, T.J., Utikal, J., and Umansky, V. (2020). Eosinophil accumulation predicts response to melanoma treatment with immune checkpoint inhibitors. Oncoimmunology 9, 1727116. 10.1080/2162402X.2020.1727116.

20.   Delyon, J., Mateus, C., Lefeuvre, D., Lanoy, E., Zitvogel, L., Chaput, N., Roy, S., Eggermont, A.M., Routier, E., and Robert, C. (2013). Experience in daily practice with ipilimumab for the treatment of patients with metastatic melanoma: an early increase in lymphocyte and eosinophil counts is associated with improved survival. Ann Oncol 24, 1697-1703. 10.1093/annonc/mdt027.

21.   Gebhardt, C., Sevko, A., Jiang, H., Lichtenberger, R., Reith, M., Tarnanidis, K., Holland-Letz, T., Umansky, L., Beckhove, P., Sucker, A., et al. (2015). Myeloid Cells and Related Chronic Inflammatory Factors as Novel Predictive Markers in Melanoma Treatment with Ipilimumab. Clinical Cancer Research 21, 5453-5459. 10.1158/1078-0432.Ccr-15-0676.

22.   Alves, A., Dias, M., Campainha, S., and Barroso, A. (2021). Peripheral blood eosinophilia may be a prognostic biomarker in non-small cell lung cancer patients treated with immunotherapy. J Thorac Dis 13, 2716-2727. 10.21037/jtd-20-3525.

23.   Okauchi, S., Shiozawa, T., Miyazaki, H., Nishino, K., Sasatani, Y., Ohara, G., Kagohashi, K., Sato, S., Kodama, T., Satoh, H., and Hizawa, N. (2021). Association between peripheral eosinophils and clinical outcomes in patients with non-small cell lung cancer treated with immune checkpoint inhibitors. Pol Arch Intern Med 131, 152-160. 10.20452/pamw.15776.

24.   Verhaart, S.L., Abu-Ghanem, Y., Mulder, S.F., Oosting, S., Van Der Veldt, A., Osanto, S., Aarts, M.J.B., Houtsma, D., Peters, F.P.J., Groenewegen, G., et al. (2020). Real-world Data of Nivolumab for Patients With Advanced Renal Cell Carcinoma in the Netherlands: An Analysis of Toxicity, Efficacy, and Predictive Markers. Clin Genitourin Cancer. 10.1016/j.clgc.2020.10.003.

25.   Zheng, X., Zhang, N., Qian, L., Wang, X., Fan, P., Kuai, J., Lin, S., Liu, C., Jiang, W., Qin, S., et al. (2020). CTLA4 blockade promotes vessel normalization in breast tumors via the accumulation of eosinophils. Int J Cancer 146, 1730-1740. 10.1002/ijc.32829.

26.   Coffelt, S.B., Kersten, K., Doornebal, C.W., Weiden, J., Vrijland, K., Hau, C.S., Verstegen, N.J.M., Ciampricotti, M., Hawinkels, L., Jonkers, J., and de Visser, K.E. (2015). IL-17-producing γδ T cells and neutrophils conspire to promote breast cancer metastasis. Nature 522, 345-348. 10.1038/nature14282.

27.   Salvagno, C., Ciampricotti, M., Tuit, S., Hau, C.S., van Weverwijk, A., Coffelt, S.B., Kersten, K., Vrijland, K., Kos, K., Ulas, T., et al. (2019). Therapeutic targeting of macrophages enhances chemotherapy efficacy by unleashing type I interferon response. Nature cell biology 21, 511-521. 10.1038/s41556-019-0298-1.

28.   Voorwerk, L., Slagter, M., Horlings, H.M., Sikorska, K., van de Vijver, K.K., de Maaker, M., Nederlof, I., Kluin, R.J.C., Warren, S., Ong, S., et al. (2019). Immune induction strategies in metastatic triple-negative breast cancer to enhance the sensitivity to PD-1 blockade: the TONIC trial. Nat Med 25, 920-928. 10.1038/s41591-019-0432-4.

29.   Theelen, W., Peulen, H.M.U., Lalezari, F., van der Noort, V., de Vries, J.F., Aerts, J., Dumoulin, D.W., Bahce, I., Niemeijer, A.N., de Langen, A.J., et al. (2019). Effect of Pembrolizumab After Stereotactic Body Radiotherapy vs Pembrolizumab Alone on Tumor Response in Patients With Advanced Non-Small Cell Lung Cancer: Results of the PEMBRO-RT Phase 2 Randomized Clinical Trial. JAMA Oncol 5, 1276-1282. 10.1001/jamaoncol.2019.1478.

30.   Chalabi, M., Fanchi, L.F., Dijkstra, K.K., den Berg, J.G., Aalbers, A.G., Sikorska, K., Lopez-Yurda, M., Grootscholten, C., Beets, G.L., Snaebjornsson, P., et al. (2020). Neoadjuvant immunotherapy leads to pathological responses in MMR-proficient and MMR-deficient early-stage colon cancers. Nature Medicine 26, 566-576. 10.1038/s41591-020-0805-8.

31.   van der Velden, D.L., Hoes, L.R., van der Wijngaart, H., van Henegouwen, B.J.M., van Werkhoven, E., Roepman, P., Schilsky, R.L., de Leng, W.W.J., Huitema, A.D.R., Nuijen, B., et al. (2019). The Drug Rediscovery protocol facilitates the expanded use of existing anticancer drugs. Nature 574, 127-131. 10.1038/s41586-019-1600-x.

32.   Kikly, K.K., Bochner, B.S., Freeman, S.D., Tan, K.B., Gallagher, K.T., D'Alessio K, J., Holmes, S.D., Abra-

hamson, J.A., Erickson-Miller, C.L., Murdock, P.R., et al. (2000). Identification of SAF-2, a novel siglec expressed on eosinophils, mast cells, and basophils. J Allergy Clin Immunol 105, 1093-1100. 10.1067/mai.2000.107127.

33. Ayers, M., Lunceford, J., Nebozhyn, M., Murphy, E., Loboda, A., Kaufman, D.R., Albright, A., Cheng, J.D., Kang, S.P., Shankaran, V., et al. (2017). IFN-gamma-related mRNA profile predicts clinical response to PD-1 blockade. The Journal of clinical investigation 127, 2930-2940. 10.1172/jci91190.

34. Derksen, P.W., Liu, X., Saridin, F., van der Gulden, H., Zevenhoven, J., Evers, B., van Beijnum, J.R., Griffioen, A.W., Vink, J., Krimpenfort, P., et al. (2006). Somatic inactivation of E-cadherin and p53 in mice leads to metastatic lobular mammary carcinoma through induction of anoikis resistance and angiogenesis. Cancer cell 10, 437-449. 10.1016/j.ccr.2006.09.013.

35. Doornebal, C.W., Klarenbeek, S., Braumuller, T.M., Klijn, C.N., Ciampricotti, M., Hau, C.S., Hollmann, M.W., Jonkers, J., and de Visser, K.E. (2013). A preclinical mouse model of invasive lobular breast cancer metastasis. Cancer research 73, 353-363. 10.1158/0008-5472.Can-11-4208.

36. Beyranvand Nejad, E., van der Sluis, T.C., van Duikeren, S., Yagita, H., Janssen, G.M., van Veelen, P.A., Melief, C.J., van der Burg, S.H., and Arens, R. (2016). Tumor Eradication by Cisplatin Is Sustained by CD80/86-Mediated Costimulation of CD8+ T Cells. Cancer Res 76, 6017-6029. 10.1158/0008-5472.CAN-16-0881.

37. Nolan, E., Savas, P., Policheni, A.N., Darcy, P.K., Vaillant, F., Mintoff, C.P., Dushyanthen, S., Mansour, M., Pang, J.B., Fox, S.B., et al. (2017). Combined immune checkpoint blockade as a therapeutic strategy for BRCA1-mutated breast cancer. Sci Transl Med 9, eaal4922. 10.1126/scitranslmed.aal4922.

38. Grimaldi, A., Cammarata, I., Martire, C., Focaccetti, C., Piconese, S., Buccilli, M., Mancone, C., Buzzacchino, F., Berrios, J.R.G., D'Alessandris, N., et al. (2020). Combination of chemotherapy and PD-1 blockade induces T cell responses to tumor non-mutated neoantigens. Commun Biol 3, 85. 10.1038/s42003-020-0811-x.

39. Wan, S., Pestka, S., Jubin, R.G., Lyu, Y.L., Tsai, Y.C., and Liu, L.F. (2012). Chemotherapeutics and radiation stimulate MHC class I expression through elevated interferon-beta signaling in breast cancer cells. PLoS One 7, e32542. 10.1371/journal.pone.0032542.

40. Cheng, J.N., Luo, W., Sun, C., Jin, Z., Zeng, X., Alexander, P.B., Gong, Z., Xia, X., Ding, X., Xu, S., et al. (2021). Radiation-induced eosinophils improve cytotoxic T lymphocyte recruitment and response to immunotherapy. Sci Adv 7, eabc7609. 10.1126/sciadv.abc7609.

41. Zimmermann, N., McBride, M.L., Yamada, Y., Hudson, S.A., Jones, C., Cromie, K.D., Crocker, P.R., Rothenberg, M.E., and Bochner, B.S. (2008). Siglec-F antibody administration to mice selectively reduces blood and tissue eosinophils. Allergy 63, 1156-1163. 10.1111/j.1398-9995.2008.01709.x.

42. Pfirschke, C., Engblom, C., Gungabeesoon, J., Lin, Y., Rickelt, S., Zilionis, R., Messemaker, M., Siwicki, M., Gerhard, G.M., Kohl, A., et al. (2020). Tumor-Promoting Ly-6G(+) SiglecF(high) Cells Are Mature and Long-Lived Neutrophils. Cell Rep 32, 108164. 10.1016/j.celrep.2020.108164.

43. Iwasaki, H., Mizuno, S., Mayfield, R., Shigematsu, H., Arinobu, Y., Seed, B., Gurish, M.F., Takatsu, K., and Akashi, K. (2005). Identification of eosinophil lineage-committed progenitors in the murine bone marrow. J Exp Med 201, 1891-1897. 10.1084/jem.20050548.

44. Pelaia, C., Paoletti, G., Puggioni, F., Racca, F., Pelaia, G., Canonica, G.W., and Heffler, E. (2019). Interleukin-5 in the Pathophysiology of Severe Asthma. Front Physiol 10, 1514. 10.3389/fphys.2019.01514.

45. Voabil, P., de Bruijn, M., Roelofsen, L.M., Hendriks, S.H., Brokamp, S., van den Braber, M., Broeks, A., Sanders, J., Herzig, P., Zippelius, A., et al. (2021). An ex vivo tumor fragment platform to dissect response to PD-1 blockade in cancer. Nat Med 27, 1250-1261. 10.1038/s41591-021-01398-3.

46. Kaptein, P., Jacoberger-Foissac, C., Dimitriadis, P., Voabil, P., de Bruijn, M., Brokamp, S., Reijers, I., Versluis, J., Nallan, G., Triscott, H., et al. (2022). Addition of interleukin-2 overcomes resistance to neoadjuvant CTLA4 and PD1 blockade in ex vivo patient tumors. Sci Transl Med 14, eabj9779. 10.1126/scitranslmed.abj9779.

47. Kos, K., Aslam, M.A., van de Ven, R., Wellenstein, M.D., Pieters, W., van Weverwijk, A., Duits, D.E.M., van Pul, K., Hau, C.S., Vrijland, K., et al. (2022). Tumor-educated T(regs) drive organ-specific metastasis in breast cancer by impairing NK cells in the lymph node niche. Cell Rep 38, 110447. 10.1016/j.celrep.2022.110447.

48. Chan, B.C.L., Lam, C.W.K., Tam, L.S., and Wong, C.K. (2019). IL33: Roles in Allergic Inflammation and Therapeutic Perspectives. Front Immunol 10, 364. 10.3389/fimmu.2019.00364.

49. Cherry, W.B., Yoon, J., Bartemes, K.R., Iijima, K., and Kita, H. (2008). A novel IL-1 family cytokine, IL-33,

potently activates human eosinophils. J Allergy Clin Immunol 121, 1484-1490. 10.1016/j.jaci.2008.04.005.

50. Suzukawa, M., Koketsu, R., Iikura, M., Nakae, S., Matsumoto, K., Nagase, H., Saito, H., Matsushima, K., Ohta, K., Yamamoto, K., and Yamaguchi, M. (2008). Interleukin-33 enhances adhesion, CD11b expression and survival in human eosinophils. Lab Invest 88, 1245-1253. 10.1038/labinvest.2008.82.

51. Johnston, L.K., and Bryce, P.J. (2017). Understanding Interleukin 33 and Its Roles in Eosinophil Development. Front Med (Lausanne) 4, 51. 10.3389/fmed.2017.00051.

52. Shani, O., Vorobyov, T., Monteran, L., Lavie, D., Cohen, N., Raz, Y., Tsarfaty, G., Avivi, C., Barshack, I., and Erez, N. (2020). Fibroblast-Derived IL33 Facilitates Breast Cancer Metastasis by Modifying the Immune Microenvironment and Driving Type 2 Immunity. Cancer Res 80, 5317-5329. 10.1158/0008-5472.can-20-2116.

53. Lucarini, V., Ziccheddu, G., Macchia, I., La Sorsa, V., Peschiaroli, F., Buccione, C., Sistigu, A., Sanchez, M., Andreone, S., D'Urso, M.T., et al. (2017). IL-33 restricts tumor growth and inhibits pulmonary metastasis in melanoma-bearing mice through eosinophils. Oncoimmunology 6, e1317420. 10.1080/2162402X.2017.1317420.

54. Holgado, A., Braun, H., Van Nuffel, E., Detry, S., Schuijs, M.J., Deswarte, K., Vergote, K., Haegman, M., Baudelet, G., Haustraete, J., et al. (2019). IL-33trap is a novel IL-33-neutralizing biologic that inhibits allergic airway inflammation. J Allergy Clin Immunol 144, 204-215. 10.1016/j.jaci.2019.02.028.

55. Ling, M.F., and Luster, A.D. (2016). Allergen-Specific CD4(+) T Cells in Human Asthma. Ann Am Thorac Soc 13 Suppl 1, S25-30. 10.1513/AnnalsATS.201507-431MG.

56. Rosskopf, S., Jahn-Schmid, B., Schmetterer, K.G., Zlabinger, G.J., and Steinberger, P. (2018). PD-1 has a unique capacity to inhibit allergen-specific human CD4(+) T cell responses. Sci Rep 8, 13543. 10.1038/s41598-018-31757-z.

57. Gorski, S.A., Lawrence, M.G., Hinkelman, A., Spano, M.M., Steinke, J.W., Borish, L., Teague, W.G., and Braciale, T.J. (2019). Expression of IL-5 receptor alpha by murine and human lung neutrophils. PLoS One 14, e0221113. 10.1371/journal.pone.0221113.

58. Kolbeck, R., Kozhich, A., Koike, M., Peng, L., Andersson, C.K., Damschroder, M.M., Reed, J.L., Woods, R., Dall'acqua, W.W., Stephens, G.L., et al. (2010). MEDI-563, a humanized anti-IL-5 receptor alpha mAb with enhanced antibody-dependent cell-mediated cytotoxicity function. J Allergy Clin Immunol 125, 1344-1353.e1342. 10.1016/j.jaci.2010.04.004.

59. Dent, L.A., Strath, M., Mellor, A.L., and Sanderson, C.J. (1990). Eosinophilia in transgenic mice expressing interleukin 5. J Exp Med 172, 1425-1431. 10.1084/jem.172.5.1425.

60. Johnston, L.K., Hsu, C.L., Krier-Burris, R.A., Chhiba, K.D., Chien, K.B., McKenzie, A., Berdnikovs, S., and Bryce, P.J. (2016). IL-33 Precedes IL-5 in Regulating Eosinophil Commitment and Is Required for Eosinophil Homeostasis. J Immunol 197, 3445-3453. 10.4049/jimmunol.1600611.

61. Pichery, M., Mirey, E., Mercier, P., Lefrancais, E., Dujardin, A., Ortega, N., and Girard, J.P. (2012). Endogenous IL-33 is highly expressed in mouse epithelial barrier tissues, lymphoid organs, brain, embryos, and inflamed tissues: in situ analysis using a novel Il-33-LacZ gene trap reporter strain. J Immunol 188, 3488-3495. 10.4049/jimmunol.1101977.

62. Hung, L.Y., Tanaka, Y., Herbine, K., Pastore, C., Singh, B., Ferguson, A., Vora, N., Douglas, B., Zullo, K., Behrens, E.M., et al. (2020). Cellular context of IL-33 expression dictates impact on anti-helminth immunity. Sci Immunol 5. 10.1126/sciimmunol.abc6259.

63. Taniguchi, S., Elhance, A., Duzer, A.V., Kumar, S., Leitenberger, J.J., and Oshimori, N. (2020). Tumor-initiating cells establish an IL-33-TGF--niche signaling loop to promote cancer progression. Science 369, eaay1813. doi:10.1126/science.aay1813.

64. Saikumar Jayalatha, A.K., Hesse, L., Ketelaar, M.E., Koppelman, G.H., and Nawijn, M.C. (2021). The central role of IL-33/IL-1RL1 pathway in asthma: From pathogenesis to intervention. Pharmacol Ther 225, 107847. 10.1016/j.pharmthera.2021.107847.

65. Jacquelot, N., Seillet, C., Wang, M., Pizzolla, A., Liao, Y., Hediyeh-Zadeh, S., Grisaru-Tal, S., Louis, C., Huang, Q., Schreuder, J., et al. (2021). Blockade of the co-inhibitory molecule PD-1 unleashes ILC2-dependent antitumor immunity in melanoma. Nat Immunol 22, 851-864. 10.1038/s41590-021-00943-z.

66. Chen, L., Sun, R., Xu, J., Zhai, W., Zhang, D., Yang, M., Yue, C., Chen, Y., Li, S., Turnquist, H., et al. (2020). Tumor-Derived IL33 Promotes Tissue-Resident CD8(+) T Cells and Is Required for Checkpoint Blockade Tumor Immunotherapy. Cancer Immunol Res 8, 1381-1392. 10.1158/2326-6066.cir-19-1024.

67. Shen, J.X., Liu, J., and Zhang, G.J. (2018). Interleukin-33 in Malignancies: Friends or Foes? Front Immunol 9,

3051. 10.3389/fimmu.2018.03051.

68. Dasari, S., and Tchounwou, P.B. (2014). Cisplatin in cancer therapy: molecular mechanisms of action. Eur J Pharmacol *740*, 364-378. 10.1016/j.ejphar.2014.07.025.

69. de Biasi, A.R., Villena-Vargas, J., and Adusumilli, P.S. (2014). Cisplatin-induced antitumor immunomodu-lation: a review of preclinical and clinical evidence. Clin Cancer Res *20*, 5384-5391. 10.1158/1078-0432.CCR-14-1298.

70. Jacobsen, E.A., Zellner, K.R., Colbert, D., Lee, N.A., and Lee, J.J. (2011). Eosinophils regulate dendritic cells and Th2 pulmonary immune responses following allergen provocation. J Immunol *187*, 6059-6068. 10.4049/jimmunol.1102299.

71. Kanda, A., Fleury, S., Kobayashi, Y., Tomoda, K., Julia, V., and Dombrowicz, D. (2015). Th2-activated eosin-ophils release Th1 cytokines that modulate allergic inflammation. Allergol Int *64 Suppl*, S71-73. 10.1016/j.alit.2015.03.006.

72. Jacobsen, E.A., Ochkur, S.I., Pero, R.S., Taranova, A.G., Protheroe, C.A., Colbert, D.C., Lee, N.A., and Lee, J.J. (2008). Allergic pulmonary inflammation in mice is dependent on eosinophil-induced recruitment of effector T cells. J Exp Med *205*, 699-710. 10.1084/jem.20071840.

73. Ghebeh, H., Elshenawy, M.A., AlSayed, A.D., and Al-Tweigeri, T. (2022). Peripheral blood eosinophil count is associated with response to chemoimmunotherapy in metastatic triple-negative breast cancer. Immu-notherapy *14*, 189-199. 10.2217/imt-2021-0149.

74. de Visser, K.E., Korets, L.V., and Coussens, L.M. (2005). De novo carcinogenesis promoted by chronic inflammation is B lymphocyte dependent. Cancer Cell *7*, 411-423. 10.1016/j.ccr.2005.04.014.

75. Kim, J.M., Rasmussen, J.P., and Rudensky, A.Y. (2007). Regulatory T cells prevent catastrophic autoimmu-nity throughout the lifespan of mice. Nat Immunol *8*, 191-197. 10.1038/ni1428.

76. Eisenhauer, E.A., Therasse, P., Bogaerts, J., Schwartz, L.H., Sargent, D., Ford, R., Dancey, J., Arbuck, S., Gwyther, S., Mooney, M., et al. (2009). New response evaluation criteria in solid tumours: revised RE-CIST guideline (version 1.1). European journal of cancer (Oxford, England : 1990) *45*, 228-247. 10.1016/j.ejca.2008.10.026.

77. Seymour, L., Bogaerts, J., Perrone, A., Ford, R., Schwartz, L.H., Mandrekar, S., Lin, N.U., Litiere, S., Dancey, J., Chen, A., et al. (2017). iRECIST: guidelines for response criteria for use in trials testing immunothera-peutics. Lancet Oncol *18*, e143-e152. 10.1016/S1470-2045(17)30074-8.

78. Picelli, S., Faridani, O.R., Björklund, A.K., Winberg, G., Sagasser, S., and Sandberg, R. (2014). Full-length RNA-seq from single cells using Smart-seq2. Nat Protoc *9*, 171-181. 10.1038/nprot.2014.006.

79. Dobin, A., Davis, C.A., Schlesinger, F., Drenkow, J., Zaleski, C., Jha, S., Batut, P., Chaisson, M., and Gingeras, T.R. (2013). STAR: ultrafast universal RNA-seq aligner. Bioinformatics *29*, 15-21. 10.1093/bioinformatics/bts635.

80. Love, M.I., Huber, W., and Anders, S. (2014). Moderated estimation of fold change and dispersion for RNA-seq data with DESeq2. Genome Biology *15*, 550. 10.1186/s13059-014-0550-8.

81. pandas, D.t. (2020). pandas-dev/pandas: Pandas. Zenodo. h10.5281/zenodo.3509134.

82. McKinney, W. (2010). Data Structures for Statistical Computing in Python from Proceedings of the 9th Python in Science Conference, 56 - 61. 10.25080/Majora-92bf1922-00a.

83. Harris, C.R., Millman, K.J., van der Walt, S.J., Gommers, R., Virtanen, P., Cournapeau, D., Wieser, E., Tay-lor, J., Berg, S., Smith, N.J., et al. (2020). Array programming with NumPy. Nature *585*, 357-362. 10.1038/s41586-020-2649-2.

84. Hunter, J.D. (2007). Matplotlib: A 2D Graphics Environment. Computing in Science & Engineering *9*, 90-95. 10.1109/MCSE.2007.55.

85. Waskom, M., Botvinnik, O., O'Kane, D., P., H., Lukauskas, S., Gemperline, D.C., Augspurger, T., Halchen-ko, Y., Cole, J.B., Warmenhoven, J., et al. (2017). mwaskom/seaborn: v0.8.1 (September 2017). Zenodo. 10.5281/zenodo.883859

86. Weber, M. (2020). statannot 0.2.2.

87. Tateno, H., Crocker, P.R., and Paulson, J.C. (2005). Mouse Siglec-F and human Siglec-8 are functionally convergent paralogs that are selectively expressed on eosinophils and recognize 6'-sulfo-sialyl Lewis X as a preferred glycan ligand. Glycobiology *15*, 1125-1135. 10.1093/glycob/cwi097.

88. Abu-Ghazaleh, R.I., Dunnette, S.L., Loegering, D.A., Checkel, J.L., Kita, H., Thomas, L.L., and Gleich, G.J. (1992). Eosinophil granule proteins in peripheral blood granulocytes. J Leukoc Biol *52*, 611-618. 10.1002/jlb.52.6.611.

89. Mori, Y., Iwasaki, H., Kohno, K., Yoshimoto, G., Kikushige, Y., Okeda, A., Uike, N., Niiro, H., Takenaka, K., Nagafuji, K., et al. (2009). Identification of the human eosinophil lineage-committed progenitor: revision of phenotypic definition of the human common myeloid progenitor. J Exp Med *206*, 183-193. 10.1084/jem.20081756.

90. Hochstetter, R., Dobos, G., Kimmig, D., Dulkys, Y., Kapp, A., and Elsner, J. (2000). The CC chemokine recep-tor 3 CCR3 is functionally expressed on eosinophils but not on neutrophils. Eur J Immunol *30*, 2759-2764. 10.1002/1521-4141(200010)30:10<2759::AID-IMMU2759>3.0.CO;2-A.

91. Alcover, A., Alarcón, B., and Di Bartolo, V. (2018). Cell Biology of T Cell Receptor Expression and Regulati-on. Annu Rev Immunol *36*, 103-125. 10.1146/annurev-immunol-042617-053429.

92. Li, Y., Yin, Y., and Mariuzza, R.A. (2013). Structural and biophysical insights into the role of CD4 and CD8 in T cell activation. Frontiers in immunology *4*, 206. 10.3389/fimmu.2013.00206.

7